IL-1β is involved in temperature-associated changes in synaptic plasticity in mouse hippocampal slices

F.M. Ross, S.M. Allan, D. Bristow, N.J. Rothwell and A. Verkhratsky

University of Manchester, School of Biological Sciences, 1.124 Stopford Building, Oxford Road, Manchester M13 9PT, UK

The temperature at which *in vitro* electrophysiological experiments are performed varies widely between laboratories. Recently it was shown that the production of cytokines within brain slices is dependent upon incubation temperature (Blond *et al.* 2001). The pro-inflammatory cytokine interleukin-1β (IL-1β) exerts a number of neuromodulatory effects in the CNS. Therefore the aim of our study was to investigate the temperature dependency of cytokine production and synaptic plasticity in slices of hippocampus.

Field excitatory postsynaptic potentials (fEPSPs) were recorded from the CA1 region of hippocampal slices prepared from C56BL/6 mice (21–35 days old; animals were killed according to UK legislation). Slices were incubated in normal ACSF either at room temperature (22–24 °C) or at 33–35 °C for at least 60 min in a holding chamber gassed with 95 % O_2 and 5 % CO_2. To measure cytokine production hippocampal slices were incubated at room temperature or at 35 °C for 3 h. Specific ELISAs determined immunoreactive IL-1β and IL-6 levels in tissue and bathing ACSF. In electrophysiology experiments the perfusing ACSF was either at room temperature or 34–35 °C. LTP was induced using a theta-burst stimulation protocol (5 trains of 15 bursts, each consisting of 4 pulses at 100 Hz with an inter-burst interval of 200 ms with the trains given at 0.1 Hz). IL-1β and IL-1ra were added to the perfusing medium for periods of 30 and 45 min, respectively. Data are expressed as means ± S.E.M. Statistical analysis was done using Student's paired *t* test within groups and ANOVA between groups. $P < 0.05$ was taken to be significant.

Hippocampal slices incubated for 3 h at 35 °C had increased IL-1β levels when compared with slices incubated at room temperature (64 ± 14 and 8 ± 1 pg ml^{-1}, respectively, $P < 0.01$, $n = 4$). There was no difference in the amount of IL-6 in hippocampal slices incubated either at 35 °C or room temperature (17 ± 3 and 16 ± 3 pg ml^{-1}, respectively).

The magnitude of LTP induced did not significantly differ at 60 min between the two temperatures. However, at 35 °C there was an initial peak 5–10 min after the tetanus had been given, which was not seen at room temperature (374 ± 51 % of control at 35 °C, $n = 4$ *versus* 172 ± 18 % at room temperature, $n = 3$, $P < 0.05$). Perfusion of IL-1ra (1000 and 2000 ng ml^{-1}) reduced this initial peak and dose-dependently reduced the extent of the resulting LTP. Perfusion with IL-1β (10 ng ml^{-1}) prior to the tetanus produced an initial increase in fEPSP slope, which was not different from under control conditions. However, at 60 min this potentiation had diminished such that the fEPSP was at approximately control values.

In conclusion incubation of hippocampal slices at physiological temperature (~37 °C) results in the specific production of IL-1β. This increase in endogenous IL-1β does not appear to affect the induction of LTP. However, IL-1ra significantly reduced the initial potentiation and also that at 60 min, suggesting that endogenous IL-1β may, in some way, contribute to LTP induction.

Blond, D. *et al.* (2001). *Brit. Neurosci. Assoc.* Abstract 16, 76*P*.

This research was supported by a MRC ROPA award.

All procedures accord with current UK legislation.

Use of interference reflection microscopy to monitor exocytosis and endocytosis in the presynaptic terminal of bipolar cells from the goldfish retina

Artur Llobet and Leon Lagnado

Laboratory of Molecular Biology, MRC, Cambridge, UK

The interference reflection microscopy (IRM) technique allows the direct visualization of close contacts between surface membrane and a glass coverslip, and has been used to study cell motility and membrane adhesion (Izzard & Lochner, 1976). Here we demonstrate that this technique can also be used to monitor changes in membrane area associated with exocytosis and endocytosis at a presynaptic terminal.

Depolarizing bipolar cells were isolated from the retina of humanely killed goldfish and whole-cell recordings made using an electrode placed on the soma. The area of close contact between the synaptic terminal and glass coverslip was visualized by IRM as a homogenous black region of destructive interference. This 'footprint' had an average area of ~40 μm^2 (10–15 % of the area of the terminal). Exocytosis was triggered by a step depolarization from −70 to −10 mV and images of the footprint recorded at 25 Hz.

Depolarizations of 20 ms or longer caused the area of the footprint (A_f) to expand, indicating an increase in the amount of membrane in contact with the glass. A 500 ms depolarisation increased A_f significantly by 4.6 ± 0.8 % (mean ± S.E.M., $n = 16$, Student's paired *t* test, $P < 0.01$). Immediately following repolarization, A_f recovered fully with a time constant of about 1 s. Changes in A_f were directly proportional to changes in total membrane surface area measured simultaneously using the capacitance technique. A 3 % increase in global capacitance caused a 1 % increase in A_f ($n = 3$). We conclude that changes in the area of the footprint measured by IRM are an accurate reflection of changes in membrane surface area associated with exocytosis and endocytosis.

A 5 s depolarization increased the A_f in three kinetically distinct phases. The first and most rapid phase was complete in < 80 ms and represented an increase in A_f of 0.5–1 %. The second phase was slower; A_f increased by 2 % in 2 s. During the third phase, A_f increased continuously at a rate of ~0.5 % s^{-1}. The recovery in A_f following a longer stimulus was relatively complex; often there was a brief further increase (representing exocytosis driven by residual calcium) followed by a fall with fast (τ ~1 s) and slow ($\tau > 10$ s) components. The kinetics of exocytosis and endocytosis measured by IRM were very similar to those measured in bipolar cell terminals using the capacitance technique or the membrane dye FM 1-43 (Neves & Lagnado, 1999).

The use of IRM provides some advantages over the use of the capacitance technique (Gillis, 1995). IRM allows a *continuous* monitor of increases in membrane surface area and can be applied to cells with complex morphologies.

Izzard, C.S. & Lochner, L.R. (1976). *J. Cell Sci.* **21**, 129–159.

Gillis, K.D. (1995). Techniques for membrane capacitance measurements. In *Single Channel Recording*, pp. 155–197. Plenum Press, New York.

Neves, G. & Lagnado, L. (1999). *J. Physiol.* **515**, 181–202.

All procedures accord with current UK legislation.

The role of mitogen-activated protein kinases in rat sensory nerve regeneration

M.F. Lockwood, A. Verkhratsky and P. Fernyhough

School of Biological Sciences, University of Manchester, 1.124 Stopford Building, Oxford Road, Manchester M13 9PT, UK

The mitogen-activated protein kinases (MAPKs) signal downstream from the small GTPases Rac/Rho/Cdc42 that are known to regulate axonal outgrowth from neurones. MAPKs may control sensory neurone axonal regeneration induced by nerve damage or axotomy via activation of transcription factors such as AP-1 and ATF2 and/or by direct interactions with cytoskeletal proteins. The aim of this study was to determine the role of MAPKs in sensory neurone regeneration using an *in vitro* system.

Levels of axonal regeneration in dissociated adult rat dorsal root ganglion (DRG) sensory neurone cultures were quantified by measuring total axon network and longest axon via immunocytochemistry and using the analysis program MetaMorph version 4.5. Data are expressed as means ± S.E.M. and statistical analysis was done using an ANOVA and a Tukey's or Dunnett's C *post-hoc* test.

Animals were killed according to current UK legislation. Dissociated DRG neurones were allowed to adhere and then treated with the ERK inhibitor U0126 (Promega) at a concentration of 10 μM, p38 inhibitor SB203580 (Calbiochem) at 2 μM or phosphinositide 3-kinase (PI 3-kinase) inhibitor LY294002 (Calbiochem) at 10 μM and nerve growth factor (NGF) at 10 ng ml^{-1}, then left overnight. The ERK inhibitor significantly reduced the level of the NGF-induced axonal network (2067 ± 1022 *versus* 8389 ± 2132 μm, $P < 0.001$, $n = 3$). The p38 and PI 3-kinase inhibitors did not significantly affect the level of NGF-induced axonal growth. The number of cells that responded to NGF was not affected by any inhibitor treatment.

Glial cell line-derived neurotrophic factor (GDNF) signals through a different subpopulation of neurones to NGF and can activate MAPKs. Dissociated DRG neurones were treated as above, using GDNF at a concentration of 10 ng ml^{-1}. The PI 3-kinase inhibitor significantly reduced the level of the GDNF-induced axonal network (2738.3 ± 500.5 *versus* 7941.7 ± 2169.1 μm, $P < 0.05$, $n = 4$). The p38 inhibitor did not significantly affect the level of the GDNF-induced axon network, nor did ERK inhibition. ERK inhibition did, however, cause a significant decrease in the GDNF-enhanced level of growth of the longest axon (515.6 ± 29.6 *versus* 646.1 ± 52.9 μm, $P < 0.05$, $n = 12$). Combined p38 and ERK inhibition significantly reduced the level of the GDNF-induced axon network (1955 ± 591.6 *versus* 6453.7 ± 2320.1 μm, $P < 0.05$, $n = 5$).

The results show that NGF signalling through ERK is required for maintenance of regenerative growth but not needed for initiation of axonal outgrowth. However, NGF signalling through p38 is not required for maintenance or initiation of axonal outgrowth. GDNF signalling through PI 3-kinase is required for maintenance of axon regeneration and GDNF activation of ERK enhances neurite elongation but does not affect total axon outgrowth. GDNF signalling through p38 and ERK in combination is required for maintenance and possibly initiation of regenerative axonal outgrowth.

This work was supported by BBSRC and Pfizer.

All procedures accord with current UK legislation.

Electrical properties of isolated neural stem cells from the adult rat hippocampus change upon differentiation

R. Hogg, H. Chipperfield, K. Whyte, V. Nurcombe and D.J. Adams

School of Biomedical Sciences, University of Queensland, Brisbane, Queensland 4072, Australia

The aim of this research is to characterise the way in which adult, self-renewing, neural progenitor cells (NPCs) acquire their electrical characteristics as they mature into active entities capable of forming neural networks. We have investigated the passive and active electrical properties of isolated, cloned NPCs from the adult rat hippocampus using whole-cell patch-clamp recording techniques. The expression of ionic channels and receptors were studied in both undifferentiated clonal cultures of NPCs and differentiated NPCs that were exposed to combinations of extracellular factors for 7–10 days (Chipperfield *et al.* 2002).

Undifferentiated NPCs had a resting membrane potential (E_m) of −89.3 ± 0.9 mV (mean ± S.E.M.) ($n = 24$), which changed by 57 mV/10-fold change in external K^+ concentration similar to that predicted by the Nernst equation for a K^+-sensitive electrode. Undifferentiated NPCs were electrically inexcitable as depolarizing current pulses failed to elicit action potentials. Under voltage-clamp conditions, voltage ramps from −120 to +20 mV reversed at −90 mV and exhibited marked inward rectification at negative membrane potentials, which was inhibited by bath application of 0.1 mM Ba^{2+}. Inward K^+ currents evoked by hyperpolarizing voltage steps were blocked in a time- and voltage-dependent manner by external Ba^{2+} but were insensitive to 4-aminopyridine and tetraethylammonium ions (TEA).

In contrast, differentiated NPCs were electrically excitable and exhibited phasic action potential firing in response to depolarizing current pulses. A time-dependent voltage sag was observed in response to hyperpolarizing current pulses. The E_m of differentiated NPCs was −57 ± 1.3 mV ($n = 26$) and the relationship between E_m and external K^+ concentration was fitted by the Goldman-Hodgkin-Katz voltage equation with $P_{Na}/P_K = 0.08$. The current–voltage relationship of differentiated NPCs obtained in response to slow voltage ramps showed marked outward rectification and reversed at ~−60 mV. Voltage-clamped cells held at −100 mV exhibited a transient inward current followed by a sustained outward current in response to depolarizing voltage steps. The transient inward current was abolished in the presence of 300 nM tetrodotoxin (TTX) and the outward current was inhibited by external TEA (5 mM), indicating the presence of functional voltage-dependent TTX-sensitive Na^+ and delayed rectifier K^+ channels in differentiated NPCs.

The functional expression of receptors in undifferentiated NPCs was examined in response to brief focal application ($\geqslant 100$ μM) of various neurotransmitters. In approximately 70 % (32/45) of undifferentiated NPCs, ATP and benzoylbenzoyl-ATP (BzATP) evoked an inward current at negative potentials, whereas acetylcholine, noradrenaline, glutamate and GABA failed to elicit a response ($n \geqslant 12$). ATP and BzATP also evoked a response in > 80 % of differentiated NPCs, suggesting that the activation of $P2X_7$ purinoceptors may play a significant role during differentiation of adult NPCs.

Chipperfield, H. *et al.* (2002). *Int. J. Dev. Biol.* **46**, 661–670.

Pre- and postsynaptic K^+ currents at the Calyx of Held

P.D. Dodson, M.C. Barker and I.D. Forsythe

Department of Cell Physiology and Pharmacology, University of Leicester, PO Box 138, Leicester LE1 9HN, UK

Low threshold K^+ currents (I_{LT}) activate near to resting potentials and influence action potential (AP) firing patterns. In the medial nucleus of the trapezoid body (MNTB) I_{LT} ensures generation of a single AP during each EPSC and is blocked by dendrotoxin-I (Brew & Forsythe, 1995), suggesting mediation by Kv1.1, Kv1.2 and/or Kv1.6 subunits. Here we investigate the subunit composition and function of pre- and postsynaptic low threshold K^+ currents.

Immunohistochemistry showed that Kv1.1, Kv1.2 and Kv1.6 were expressed in the MNTB, but Kv1.4 and Kv1.5 were not. Brainstem slices (100–150 μm thick) were prepared from Lister Hooded rats (P6–14) humanely killed by decapitation. Subunit-specific toxins (100 nM) were applied during whole-cell patch recordings to investigate the contribution of Kv1 subunits to I_{LT}. DTX-K, a specific blocker of channels containing Kv1.1, blocked $90 \pm 4\%$ of I_{LT} ($n = 4$, mean ± S.E.M.), whereas tityustoxin-Kα (TsTX), which blocks channels containing Kv1.2, blocked $48 \pm 4\%$ of I_{LT} ($n = 7$). Thus I_{LT} is composed of two components: one is TsTX sensitive (hence I_{LTS}) and the other is TsTX resistant (I_{LTR}). The pharmacology and histology are consistent with I_{LTS} being mediated by Kv1.1/1.2 heteromers and I_{LTR} by Kv1.1/1.6 heteromers. Block of I_{LTS} caused trains of APs on depolarisation in current clamp, suggesting that I_{LTS} is dominant in maintaining the phenotypic single AP response of MNTB neurones. One explanation for this dominance is that I_{LTS} is preferentially located at a spike initiation region in the axon. Indeed Kv1.1 and Kv1.2 (I_{LTS}) immunoreactivity was concentrated in the initial 20–30 μm of the axon, whereas Kv1.6 (I_{LTR}) could not be detected axonally ($n = 3$).

We also examined the presynaptic low threshold K^+ currents by making whole-cell recordings from the calyx. In contrast to the postsynaptic currents, TsTX blocked $87 \pm 5\%$ of the presynaptic low threshold current ($n = 7$) and increased the number of action potentials fired, whereas DTX-K had no effect.

Low threshold K^+ currents in MNTB neurones are mediated by two heteromeric Kv1 channels: I_{LTS} channels are Kv1.1/1.2 heteromers, whereas those of I_{LTR} are likely to be Kv1.1/1.6 heteromers. I_{LTS} has the dominant function in maintaining the single AP response, a property that may be conferred by its preferential localisation to the initial 20–30 μm of the axon. Presynaptic low threshold K^+ channels have a different subunit composition to postsynaptic channels, with presynaptic AP firing being governed by channels containing Kv1.2 but not Kv1.1.

Brew, H.M. & Forsythe, I.D. (1995). *J. Neurosci.* **15**, 8011–8022.

This work was supported by The Wellcome Trust.

All procedures accord with current UK legislation.

Channel noise limits the minimum diameter of axons

A. Aldo Faisal and Simon B. Laughlin

Department of Zoology, University of Cambridge, Cambridge CB2 3EJ, UK

The action potential (AP) propagates by the concerted action of voltage-gated ion channels, whose probabilistic behaviour introduces noise (Chow & White, 1996). We investigated whether these fluctuations determine the lower limit of the operational diameter in unmyelinated axons. Since recording from fine axons is technically difficult, we developed a stochastic simulator of an unmyelinated axon using a biophysically realistic model of stochastic ion channel behaviour (Faisal *et al.* 2002). It also allows us to explore the properties of unnaturally fine axons.

We simulated axons of diameters between 0.025 and 3 μm with Na and K channel densities of 60 and 18 μm^{-2}, respectively, and a single-channel conductance of 20 pS. The spontaneous AP rate goes up as the diameter is reduced (Fig. 1) because, with axoplasmic resistance proportional to diameter squared, less current is dissipated along the axon. Thus a spontaneously activated channel can depolarise the membrane to threshold if it remains open long enough to charge the membrane capacitance.

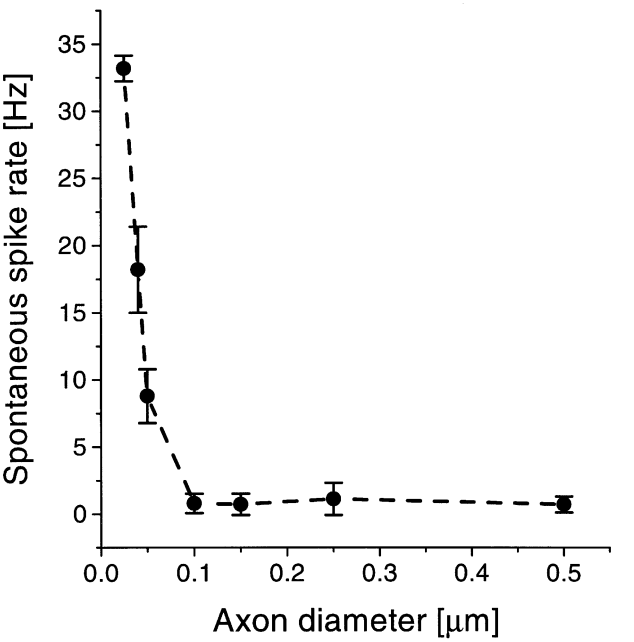

Figure 1. Spontaneous AP rate *vs.* diameter in 1 mm long unmyelinated axons at 6.3°C ($n = 10$, bars are ± S.D.).

Below a critical diameter of 0.1 μm the axon can be driven to AP threshold by a single ion channel, to produce spontaneous AP rates > 5 Hz. We verified that this effect is insensitive to specific channel densities, by doubling and halving the densities independently.

The critical diameter 0.1 μm relates well to anatomical data, as the thinnest known fibres are 0.1 μm in diameter (Berthold, 1978).

Berthold, C.-H. (1978). In *Physiology and Pathobiology of Axons,* ed. Waxman, S.G., pp. 3–63. Raven Press, NY.

Chow, C.C. & White, J.A. (1996). *Biophys. J.* **71**, 3012–3021.

Faisal, A.A. *et al.* (2002). *Proc. Intl. Joint Conf. Neural Networks,* pp. 1661–1666. IEEE, Honolulu, HI.

A.A.F. is supported by a Boehringer-Ingelheim Fonds PhD Fellowship and the BBSRC.

The effects of oleamide and cannabinoids on the induction of long-term potentiation (LTP) in the CA1 region of the rat hippocampal slice by two different patterns of stimulation

George Lees and Antonios Dougalis

Institute of Pharmacy and Chemistry, School of Sciences, University of Sunderland, Sunderland SR1 3SD, UK

Cannabinoids, whether naturally occurring (Δ9-THC), synthetic (WIN55212-2) or endogenous (anandamide, 2-AG) have all been shown to disrupt hippocampal LTP (Terranova *et al.* 1995; Stella *et al.* 1997). Oleamide (cOA) is a brain lipid with sleep-inducing properties that are blocked by the CB1 receptor antagonist SR141716A (Mendelson & Basile, 1999). Here we examine the effects of the putative endocannabinoid on the induction of LTP in rat brain slices.

Male Wistar rats (150–200 g) were humanely killed and transverse slices (400 μm) containing the hippocampus were obtained. After 1 h recovery, slices were perfused (2–3 ml min^{-1}) with ACSF (composition (mM): NaCl 124, KCl 3, $MgCl_2$ 1, $CaCl_2$ 2, $NaHCO_3$ 26, NaH_2PO_4 1.25 and D-glucose 10, equilibrated with carbogen) at 35 °C. ACSF was supplemented with 0.1 % BSA and 0.1 % DMSO in all experiments to aid drug dissolution. Extracellular field potentials (fEPSP) were obtained from the stratum radiatum in response to stimulation of the Schaffer's collaterals (0.1 ms pulses, 0.05 Hz). We assessed synaptic modulation as changes in the initial slope (20–80 % of maximum amplitude of the fEPSP) of the recorded signal. fEPSP values are expressed as % mean ± S.E.M. (normalised to pretreatment). Statistical tests are as stated below. A P value of < 0.05 was judged significant.

HFS (high frequency stimulation, 100 Hz for 1 s repeated after 20 s) predictably increased the slope of the fEPSP 30 min after stimulation in the absence of drugs (191 ± 24 *vs.* control baseline, $P < 0.01$, paired t test, $n = 5$), while θ-burst (10 trains of 4 bursts at 100 Hz delivered 200 ms apart), given 30 min post-HFS, caused a smaller further incremental increase in fEPSP slope measured a further 30 min later (132 ± 5 *vs.* pre-θ baseline, paired t test, $P > 0.05$, $n = 5$). Neither 32 μM cOA nor 10 μM anandamide significantly altered the fEPSP slope during pre-incubation in ACSF, prior to high frequency stimulation, but WIN55212-2 (5 μM) depressed fEPSP amplitude and slope (59 ± 4.5 of control, $n = 4$, $P < 0.01$, paired t test). WIN55212-2 (5 μM) reliably, and potently, inhibited both HFS and θ-burst LTP induction (HFS 104.5 ± 4.856, θ-burst 105.0 ± 5.845, $n = 4$, unpaired t tests, $P < 0.001$). Anandamide (10 μM), significantly attenuated responses to HFS-induced LTP, but failed to block θ-burst-LTP (HFS 130.0 ± 13.05, $P < 0.05$, θ-burst 139.8 ± 13.92, $P > 0.05$, $n = 5$, unpaired t tests). Oleamide (32 μM) did not block HFS-LTP but attenuated θ-burst-LTP (HFS 174.5 ± 22.91 $P < 0.05$, θ-burst 109.5 ± 4.406, $P > 0.05$, $n = 4$, unpaired t tests).

Oleamide does not profoundly and indiscriminately occlude LTP as seen with synthetic cannabinoid agonists. The different profiles observed with endocannabinoids may reflect mechanisms of action, but differential lipophilicity, permeation and metabolism within the slice complicate this issue.

Mendelson, W.B. & Basile, A.S. (1999). *NeuroReport* **10**, 3237–3239.

Stella, N. *et al.* (1997). *Nature* **388**, 773–778.

Terranova, J.P. *et al.* (1995). *Naunyn–Schmiedeberg's Arch. Pharmacol.* **352**, 576–579.

This work was supported by The Wellcome Trust, College of Pharmacy Practice, RPharm Soc GB and NI.

All procedures accord with UK legislation.

Endogenous cannabinoids decrease mIPSC frequency in rat cortical neurones in culture

Leanne Coyne and George Lees

University of Sunderland, Wharcliffe Street, Sunderland SR1 3SD, UK

The synthetic cannabinoid WIN 55212-2 reduces the frequency of miniature inhibitory postsynaptic currents (mIPSCs) in brain slices, but the identity of the endogenous messenger underpinning DSI (despolarisation-induced suppression of inhibition) is unknown (Wilson & Nicoll, 2001). Here we compare the effects of synthetic CB1 agonists with endocannabinoid candidates on mIPSCs in cultured monolayers in the absence of permeability and metabolic barriers.

Culture techniques and saline composition have been published previously (Nicholson *et al.* 2001). Cells were whole-cell patch-clamped at 22–24 °C. All solutions contained 0.1 % dimethylsulphoxide (vehicle) and 0.1 % bovine serum albumin. To isolate mIPSCs, 200 nM tetrodotoxin, 2 μM CNQX and 10 μM D-AP5, 2 mM Mg^{2+} and 0.5 mM Ca^{2+} were included. Intracellular saline contained (mM) $CsCl_2$ (132), $CaCl_2$ (1), $MgCl_2$ (2), Hepes (10) and EGTA (11); pH 7.4. Data were analysed using Spike 2 and Prism (Graphpad) software. Data (presented as means ± S.E.M.) were analysed using a Friedman ANOVA, with a Dunn's post test. P values < 0.05 were considered significant.

In physiological saline, at a holding potential of −60 mV, WIN 55212-2 significantly reduced the frequency of mIPSCs (control, 1.54 ± 0.23 Hz; 0.8 μM WIN 55212-2, 1.03 ± 0.17 Hz; wash, 1.62 ± 0.28 Hz, $P < 0.05$, $n = 5$), consistent with effects in slices (Wilson & Nicoll, 2001). Anandamide (ANA) irreversibly mimicked this effect (control, 1.70 ± 0.41; 32 μM anandamide, 0.76 ± 0.26; wash, 0.88 ± 0.24, $P < 0.01$, $n = 6$). The CB2 ligand palmitoylethanolamide (PEA) did not depress the frequency of mIPSCs (control, 2.62 ± 0.64; 10 μM PEA, 2.49 ± 0.69; wash, 2.54 ± 0.63, $P > 0.05$). In the presence of the CB1 antagonist, AM251, the depressant effect of WIN 55212-2 was prevented (control, 1.17 ± 0.32 Hz; 0.8 μM WIN 55212-2, 1.12 ± 0.28 Hz; wash, 1.15 ± 0.27 Hz, $P > 0.05$, $n = 6$). The depressant effect of the endogenous cannabinoid, anandamide was also prevented in the presence of the CB1 antagonist AM251 (control, 0.79 ± 0.18 Hz; 32 μM ANA, 0.83 ± 0.24 Hz; wash, 0.78 ± 0.18 Hz, $P > 0.05$, $n = 5$). The sleep hormone oleamide causes an increase in mIPSC frequency (control, 0.86 ± 0.22 Hz; CoA, 2.13 ± 0.64 Hz; wash, 0.73 ± 0.15 Hz; $P < 0.05$, $n = 4$).

ANA but not PEA mimicks synthetic CB1 ligands in reducing the frequency of mIPSCs. These effects are prevented by the selective CB1 antagonist, AM251. The sleep hormone oleamide does not apear to be cannabamimetic.

Nicholson, R.A. *et al.* (2001). *Anesthesiology* **94**, 120–128.

Wilson, R.I. & Nicoll, R.A. (2001). *Nature* **410**, 588–592.

Thanks to The Wellcome Trust for financial support and to David Hills for the cell cultures.

All procedures accord with UK legislation

Synaptic rearrangements underlying map plasticity in layer 2/3 rat barrel cortex

Carl Petersen, Michael Brecht and Bert Sakmann

Max-Planck-Institute for Medical Research, Heidelberg, Germany

Activity-dependent cortical plasticity may contribute to organising the representation of sensory information in well-ordered maps. The rodent neocortical somatosensory map is exceptionally well delineated by the layer 4 barrel pattern, which is isomorphic to the layout of the whiskers on the rodent snout. These barrels can be visualised in living brain slices, allowing the neocortical circuits of specific regions of the sensory map to be investigated in detail. Activity-dependent plasticity can be induced by simply trimming whiskers.

In our experiments we trimmed whiskers belonging to rows A, B and C (sparing whiskers of rows D and E) for a period of over 10 days, beginning around a week after birth. The neuronal networks activated by the spared D row whiskers are particularly interesting to investigate since they are flanked by deprived cortex on one side (representing the trimmed C row whiskers) and spared cortex on the other (representing the spared E row whiskers). Large-scale changes in the representation of D row whiskers in layer 2/3 were investigated *in vivo* by voltage-sensitive dye (RH1691) imaging and whole-cell recordings targeted to specific barrel columns. Brief deflection of the D2 whisker in the urethane ($1.5\ g\ kg^{-1}$)-anaesthetised rat evoked responses initiating in the D2 barrel column and subsequently spreading over the barrel field. In control animals the response preferentially spread towards the C row ($n = 10$), whereas in the deprived animals responses preferentially spread to the E row ($n = 10$). To investigate in detail how the neocortical circuits are altered, barrel columns representing rows C, D and E were identified in brain slices. Voltage-sensitive dye responses evoked by electrical stimulation of a D row barrel *in vitro* were also different between control ($n = 19$) and deprived ($n = 20$) animals. The early response was columnar in both groups but subsequently the signal spread asymmetrically within layer 2/3. In deprived animals (but not in control animals) the spread was preferentially towards the E row. This result suggests that changes in the layer 2/3 neuronal network might account for a major part of the observed plasticity. Thus the connectivity of the excitatory neuronal network of layer 2/3 was investigated by simultaneously recording postsynaptically from pyramidal neurons located in the C row and E row and checking for excitatory responses evoked by action potentials in individual pyramidal neurons located in the D row. The number of synaptic connections originating from D row pyramidal neurons was highest with C row postsynaptic neurons in control animals but with E row neurons in deprived animals.

This whisker trimming protocol thus induces a reversal of the preferred connectivity of excitatory neurons in the D row layer 2/3 barrel columns. After deprivation pyramidal neurons in layer 2/3 of D row preferentially synaptically connect with pyramids in the neighbouring spared E row barrel column rather than expanding into the deprived C row cortex.

All procedures accord with current national guidelines.

Correlation between morphology and spontaneous synaptic activity of CA1 neurones during development in acute and organotypic slices

A. De Simoni, C.B. Griesinger and F.A. Edwards

Department of Physiology, Gower Street, London WC1E 6BT, UK

Patch-clamp recording of synaptic currents in acute and organotypic rat brain slices has been commonly used for studying synaptic physiology over the last decade. We have thus compared the features of spontaneous synaptic activity and the morphology of neurones in the hippocampal CA1 region in these two preparations, over the first 3 weeks of development.

We found that the number of spines and the frequency of spontaneous activity increased dramatically from P14 (postnatal day 14) to P21 in acute slices. Moreover, changes in morphology and spontaneous synaptic activity in acute slices, over this period, are fundamentally similar to those in organotypic slices DIV7 (7 days *in vitro*) to DIV21. (Acute slices, $n = 12$, t test, $P < 0.05$; organotypic slices, $n = 21$, t test, $P < 0.05$.)

Thus network development follows similar steps, whether the connections develop *in vivo* or *in vitro*, though over a slightly longer time scale in cultured tissue. This makes the organotypic slice a good model for synaptic development but underlines the importance of the time window chosen. Thus perhaps surprisingly, development is independent of experience, at least after P5 when the organotypic slices are made.

In both preparations the density of spines increases about 3-fold over the period studied. Similarly, for both acute and cultured slices the frequency of miniature excitatory postsynaptic currents (mEPSCs) also rises 3.7 and 3.4 times, respectively. (Acute slices, $n = 8$, t test, $P < 0.05$; organotypic slices, $n = 21$, t test, $P < 0.05$.) This suggests a linear relationship between the spine number and the mEPSCs of these neurones.

The one clear difference, as observed previously, is that hippocampal neurones in organotypic slices become hyperconnected (Debanne *et al.* 1995). This is reflected in an increased complexity of the dendritic tree. We used a fractal method to quantify this parameter and found that in organotypic slices CA1 neurones become richer in dendrites of the secondary and tertiary order. As the spine density is similar in both groups this results in a higher total synapse number in the organotypic slices. This increase is reflected in a higher frequency of spontaneous synaptic activity, while other parameters, such as amplitude and kinetics remain similar during development in both preparations. Overall this suggests that connectivity is greater in organotypic slices but the dendritic electrical properties are relatively unchanged.

We also studied changes in spine shape over development using confocal microscopy. The primary changes seen are a decrease in stubby spines from nearly 50 % down to about 25 %, and an increase from 25 % to 50 % in thin spines in both acute and cultured slices. The filopodia also decrease from around 15 % to 4 % in acute slices and to only 1 % in organotypics.

All the experiments conformed to current UK legislation. The animals were killed humanely.

Debanne, D. *et al.* (1995). *J. Neurophysiol.* **73**, 1282–1294.

All procedures accord with current UK legislation

Spreading depression-induced preconditioning in the cortex of mice: differential changes in the expression of nAChR and glutamate receptor subunits

P.L. Chazot*, O.V. Godukhin† and T.P. Obrenovitch†

*Pharmacology, Institute of Pharmacy, Chemistry and Biomedical Sciences, University of Sunderland, Sunderland and †Pharmacology, School of Pharmacy, University of Bradford, Bradford, UK

Cortical spreading depression (CSD) is a robust method for the induction of brain preconditioning, i.e. the adaptive cytoprotection that protects against subsequent, potentially lethal insults (Obrenovitch *et al.* 2002). We are interested in delineating the mechanisms underlying brain preconditioning with a view to identifying novel neuroprotection strategies. Recent studies have shown that reduction in cell-surface expression AMPA receptors protected primary hippocampal neurons from ischaemic stress (Ralph *et al.* 2001). In addition, up-regulation of α7 nAChRs has been proposed to explain the neuroprotection afforded by chronic nicotine treatment of neuronal cell cultures (Jonnala & Buccafusco, 2001). Here we report recent findings focusing on effects of CSD-induced preconditioning upon the glutamatergic and cholinergic systems.

All animal procedures complied with the UK Animals (Scientific Procedures) Act, 1986. Adult male C57B1/6 mice (25–30 g) were anaesthetized with halothane and placed in a stereotaxic frame. Ten full consecutive recurrent CSDs were elicited by epidural application of 1 M KCl to the right occipital cortex, as previously described (Obrenovitch *et al.* 2002). In sham-operated controls, 1 M KCl was replaced by physiological saline. Animals were re-anaesthetized 24 h later, killed by decapitation, the brain removed, and the whole hemicortices dissected out and rapidly frozen in liquid nitrogen. P_2 membranes from individual sham- and KCl-treated right hemicortices were prepared and subjected to quantitative immunoblotting (Obrenovitch *et al.* 2002). Four mice were used in each treatment group. Polyclonal anti-rodent NR1 (17–35), NR2A (1381–1394) and NR2B (46–60) antibodies (Chazot *et al.* 2002) were used at a final protein concentration of 1 μg ml^{-1}. Polyclonal anti-GluR1 and GluR2 antibodies were used at a concentration of 1/3000. Monoclonal anti-α7 nAChR subunit (Martin-Ruiz *et al.* 2000) was used at 1/5000. Loading variations were standardized by reprobing the immunoblots with monoclonal anti-β-actin antibodies (1/1000). Immunoblots were quantified by densitometry using a Gel Doc 2000 system. Optical density values (standardized with β-actin) were compared using Student's unpaired t test with a significance level of $P < 0.05$.

In comparison with the sham-treated samples, KCl treatment resulted in a modest parallel *reduction* in both GluR1 (30 ± 13 %) and GluR2 (28 ± 13 %) expression (means ± S.D., $n = 4$ of each group, $P < 0.03$). No significant changes were detected in NR1, NR2A or NR2B immunoreactivities ($n = 4$ of each group, $P > 0.05$). In marked contrast, a profound *increase* in α7 nAChR subunit expression was observed (15 ± 4-fold; mean ± S.D., $n = 4$ of each group, $P < 0.001$) following preconditioning. In conclusion, these changes in AMPA and neuronal nicotinic receptor protein expression may underlie in part the adaptive cytoprotection afforded by CSD. The anatomical profile and the physiological consequences of these changes in protein expression are currently under investigation.

Chazot, P.L. *et al.* (2002). *Neuropharmacology* **42**, 319–324.

Jonnala, R.R. & Buccafusco, J.J. (2001). *J. Neurosci. Res.* **66**, 565–572.

Martin-Ruiz, C.M. *et al.* (2000). *Neuropharmacology* **39**, 2830–2839.

Obrenovitch, T.P. *et al.* (2002). *Neurosci. Lett.* **320**, 161–163.

Ralph *et al.* (2002). *Mol. Cell. Neurosci.* **17**, 662–670.

This work was supported by the European Commission, contract no. QLG3-CT-2000-00934 and The Wellcome Trust (UK).

All procedures accord with current UK legislation.

Modulation of seizure activity by adenosine A_1 and A_{2A} receptor antagonists in the CA1 region of the rat hippocampus *in vitro*

Lori-An V. Darling and Bruno G. Frenguelli

Department of Pharmacology and Neuroscience, University of Dundee, Ninewells Hospital, Dundee DD1 9SY, UK

Adenosine is released during seizure activity where it has been described as an endogenous anticonvulsant through its ability to inhibit glutamate release via presynaptic adenosine A_1 receptors. In contrast, activation of adenosine A_{2A} receptors facilitates glutamate release. We have investigated the relative contributions of adenosine A_1 and A_{2A} receptors to seizure activity in the CA1 region of the rat.

Hippocampal slices, 600 μm thick, were prepared from rat pups of either sex aged between 17 and 22 days. Rats were killed by cervical dislocation in accordance with Schedule 1 of the UK Animals (Scientific Procedures) Act, 1986. Slices were maintained in nominally Mg^{2+}-free ACSF, bubbled with 95 % O_2 and 5 % CO_2. Field excitatory postsynaptic potentials (fEPSPs) were recorded from area CA1 with an ACSF-filled glass microelectrode in response to stimulation of stratum radiatum at 15 s intervals. Seizures were induced at 10 min intervals using a 2 s 60 Hz train of stimuli. The A_1 receptor antagonist CPT (1 μM) and the A_{2A} receptor antagonist ZM241385 (100 nM) were applied via the bath solution for at least 10 min before the first train was given. Experiments were performed at 33–34°C. Data are presented as means ± S.E.M. and n = the number of slices.

Up to six trains of stimuli were given to each slice. Under control conditions, the mean duration of the first three seizures elicited by the trains (28 ± 4 s) did not differ (paired t test; $P > 0.05$; $n = 6$) from the mean duration of the second three train-induced seizures (28 ± 5 s). Seizure activity depressed the concurrently recorded fEPSP by 62 ± 7 %. In contrast, the mean duration of the seizures elicited in the presence of CPT (37 ± 8 s; $n = 7$) was significantly greater ($P < 0.02$) than the corresponding control seizures (20 ± 4 s). CPT also greatly attenuated ($P < 0.001$) the seizure-induced depression of the fEPSP (24 ± 3 % depression) compared with controls (57 ± 5 % depression). Furthermore, the occurrence of spontaneous seizures was greater in CPT-treated slices than controls (73 *vs.* 22 % of slices, respectively). ZM241385 slightly reduced the duration of seizure activity (23 ± 4 s; $P < 0.01$; $n = 11$) compared with corresponding controls (28 ± 4 s) but had no appreciable influence on the seizure-induced depression of the fEPSP (control 75 ± 3 %; ZM241385 71 ± 5 %).

These results confirm the powerful role of endogenous adenosine, acting via A_1 receptors, in the termination of epileptiform activity in area CA1 of the hippocampus. Our data also show a small contribution to the promotion of seizure activity by adenosine A_{2A} receptors. This reduced role may reflect the lower numbers of A_{2A} receptors in area CA1.

L.V.D. is supported by the MRC.

All procedures accord with current UK legislation.

Oleamide attenuates the frequency of 4-aminopyridine (4AP)-induced spontaneous epileptiform activity in the CA3 pyramidal neurons of the rat hippocampal slice via a CB1 receptor-independent mechanism

Antonios Dougalis and George Lees

Institute of Pharmacy and Chemistry, School of Sciences, University of Sunderland, Sunderland SR1 3SD, UK

cis-Oleamide (cOA) is a brain lipid that regulates physiological sleep. It is often classified as an endocannabinoid although *in vitro* evidence for a CB1 receptor interaction is lacking (e.g. Boring *et al.* 1996). cOA is a blocker of neural Na^+ channels/burst firing (Verdon *et al.* 2000; Nicholson *et al.* 2001), it positively modulates $GABA_A$ receptors (Verdon *et al.* 2000) and it blocks gap junctions (Guan *et al.* 1997). These actions are common to anticonvulsant drugs. We address the hypothesis that cOA may be an endogenous anticonvulsant.

Male Wistar rats (*ca* 150 g) were humanely killed. ACSF (NaCl 135 mM, KCl 3, $MgCl_2$ 1, $CaCl_2$ 2, NaH_2PO_4 1.25, $NaHCO_3$ 16, glucose 10) with 4AP (100 μM) was superfused for 45 min over saggital hippocampal slices (400 μm) at 35 °C. Extracellular field recordings were obtained from the CA3c subfield. 0.1 % BSA (for cOA experiments only) and 0.1 % DMSO were added to salines containing hydrophobic ligands. Values reported below are % means ± S.E.M. (normalised to pretreatment). Statistical analysis was as stated below. A P value of < 0.05 was judged significant.

4AP perfusion resulted in the appearance of both primary, inter-ictal bursts (90–150 ms duration, all slices) and secondary (> 0.25–3 s, 3 of 49 slices) ictal-like epileptiform events in the CA3 region of the hippocampus. cOA (64 μM) and WIN55212-2 (5 μM), after 60 min, both decreased the frequency of the primary events compared with time-matched controls (cOA 71.5 ± 1.7, $n = 6$, $P < 0.001$; WIN 47.25 ± 2.5, $n = 4$, $P < 0.0001$; controls 97.50 ± 2.1, $n = 4$, unpaired t tests). Carbamazepine (CBZ 100 μM) reversibly increased the frequency of primary epileptiform events (CBZ after 30 min 147.0 ± 7.6, $n = 7$, $P < 0.001$; wash 98.0 ± 4.0, $n = 4$, $P > 0.05$; control 101.0 ± 2.2, $n = 7$, paired t tests). CBZ (320 μM) caused a very transient increase in the frequency (after 1–2 min), but then markedly reduced their incidence after 15 min of perfusion (48.75 ± 9.3, $n = 4$, $P < 0.05$; control 99.25 ± 2.529, $n = 4$, paired t test). Pre-treatment of the slices for 30 min with the selective and potent CB1 antagonist AM251 (5 μM) did not affect the ability of cOA to suppress the frequency of epileptiform activity (cOA and AM251 67.33 ± 5.2, $n = 3$, $P > 0.05$, unpaired t tests) but fully blocked the effects of WIN5512-2 (WIN55212-2 and AM251 95.41 ± 3.35, $n = 2$, $P < 0.01$). Qualitatively, all three ligands rapidly and completely blocked the ictal-like discharges at these concentrations.

Factors limiting the incidence of type II discharges in this model (highly sensitive to anticonvulsants and cOA) are poorly understood. cOA exhibits anticonvulsant effects which (unlike WIN55212-2) are not mediated via CB1 receptors.

Boring, D.L. *et al.* (1996). *Prostag. Leukotr. Ess. Fatty Ac.* **55**, 207–210.

Guan, X. *et al.* (1997). *J. Cell Biol.* **139**, 1785–1792.

Nicholson, R.A. *et al.* (2001). *Anesthesiology* **94**, 120–128.

Verdon, B. *et al.* (2000). *Br. J. Pharmacol.* **129**, 283–90.

This work was supported by The Wellcome Trust, College of Pharmacy Practice, RPharm Society of GB and NI.

All procedures accord with current UK legislation.

P2X receptor-mediated currents in the pyramidal neurones of somatosensory cortex

Yu. Pankratov*†, U. Lalo*† and A. Verkhratsky†

**Bogomoletz Institute of Physiology, Kiev, The Ukraine and* †*University of Manchester, School of Biological Sciences, 1.124 Stopford Building, Oxford Road, Manchester M13 9PT , UK*

Fast P2X receptor-mediated excitatory postsynaptic current (EPSC) was identified in the pyramidal neurones of layers II/III and V of somatosensory cortex in slices obtained from the brain of 17- to 22-day-old rats. Animals were killed according to UK legislation. The EPSCs were elicited by electrical stimulation of vertical axons originating from layer IV–VI neurones at 0.1 Hz in the presence of 20 μM bicuculline. When the glutamatergic EPSC was blocked by the saturating concentrations of glutamate receptor inhibitors NBQX and D-AP5, a small EPSC component was recorded from 90 % of neurones tested. The amplitude of residual EPSC averaged 9.7 ± 7.1 % ($n = 44$, all data are presented as means ± S.D.) of total EPSC amplitude measured at a holding potential of −80 mV. Doubling the concentration of glutamatergic antagonists did not affect the amplitude of residual EPSC (rEPSC), indicating that it was not due to incomplete inhibition of glutamate receptors, thus representing an activation of non-glutamatergic ionotropic receptors. To verify the absence of chloride conductance contribution to rEPSC we replaced caesium chloride in the intrapipette solution with caesium gluconate. Neither amplitude nor current–voltage relationship of rEPSC were changed after substitution of intracellular Cl^- ions for gluconate. The reversal potential of rEPSC recorded using the caesium gluconate-based pipette solution was 15.5 ± 4 mV ($n = 7$), the corresponding values for caesium chloride-based pipette solution was 15 ± 5 mV ($n = 7$). This result demonstrates negligible contribution of chloride conductance to rEPSC.

The rEPSC was not affected by selective blockers of nicotinic (hexamethonium) and serotonin (Y25130) receptors, although it was reversibly inhibited by antagonists of P2X receptors (NF023, NF279 and PPADS). The specific P2X receptor blocker NF023 (10 μM) reduced the amplitude of rEPSC by 73 ± 22 % ($n = 7$). The inhibitory effects of NF279 (2 μM) and PPADS (30 μM) were 61 ± 18 % ($n = 10$) and 51 ± 9 % ($n = 8$), respectively.

An application of ATP (10 μM) or α,β-methylene ATP (10 μM) to pyramidal neurones, acutely isolated from cortical slices, evoked inward currents (30–200 pA) in 65 % of cells tested. ATP-mediated currents were reversibly blocked by P2X antagonists. This inhibition was significant but not complete: PPADS (30 μM), and suramin (50 μM) reduced the amplitude of ATP-induced currents by 48 ± 8 % ($n = 6$) and 53 ± 14 % ($n = 5$), respectively. The voltage dependence of ATP-induced currents was almost similar to the purinergic rEPSC. The values of reversal potential measured at extracellular calcium concentrations of 2 and 5 mM were 12.5 ± 0.7 and 17.1 ± 1.1 mV ($n = 5$). The relative calcium permeability (P_{Ca}/P_{Cs}) of P2X receptors was 12.3 as estimated from reversal potential of ATP-induced current measured at different extracellular calcium concentrations.

We concluded that P2X purinoreceptors participate in synaptic transmission in neocortex. In cortical pyramidal neurones P2X receptors may provide a significant Ca^{2+} entry at resting membrane potentials, and hence an ATP-activated component of synaptic transmission may play an important role in cortical pyramidal neurone function.

This research was supported by The Wellcome Trust.

All procedures accord with current UK legislation.

Subunit specificity of P2X receptor trafficking

Laura K. Bobanovic, Stephen J. Royle and Ruth D. Murrell-Lagnado

Department of Pharmacology, University of Cambridge, Tennis Court Road, Cambridge CB2 1PD, UK

Novel endocytic motif for a P2X receptor

Stephen J. Royle, Laura K. Bobanovic and Ruth D. Murrell-Lagnado

Department of Pharmacology, University of Cambridge, Tennis Court Road, Cambridge CB2 1PD, UK

Constitutive recycling of ionotropic receptors between the plasma membrane to intracellular compartments allows cells to regulate the surface number of receptors by changing the relative rates of internalisation or insertion. Classically, membrane proteins that are to be endocytosed are recruited to clathrin-coated pits via interactions between YXXΦ (single amino acid code where Φ is an amino acid with a bulky, hydrophobic side chain and X is any amino acid) endocytic motifs and the medium (μ2) subunit of the AP-2 complex. The molecular details of how recycling ionotropic receptors link to the endocytic pathway, however, are poorly understood.

Previously we have shown that $P2X_4$, but not $P2X_2$ receptors are constitutively recycled in HEK293 cells and cultured neurones (Bobanovic *et al.* 2002; neonatal rats were humanely killed according to UK guidelines). Here, using chimeric $P2X_4$–$P2X_2$ receptors and deletion mutants of the $P2X_4$ receptor we found that the C-terminus of $P2X_4$ is important for trafficking. To identify which residues were involved we generated mutant $P2X_4$ receptors with alanine substitutions at various positions. Mutation of Y378, G381 and L382 inhibited internalisation of $P2X_4$ receptors expressed in cultured neurones. Surprisingly, a more conservative phenylanine substitution (Y378F) was equally as disruptive as an alanine substitution (Y378A) at position 378. Residues Y378, G381 and L382 therefore represent a non-canonical tyrosine-based endocytic motif (YXXGL) for the $P2X_4$ receptor.

Mutant receptors that were internalisation-deficient accumulated at the cell surface as assessed by antibody-labelling of surface receptors in living neurones. In addition, there was a concomitant increase in the size of the functional pool of receptors as assessed by measuring peak current densities in response to application of ATP (100 μM). Since the μ2 subunit of the AP-2 complex recognises canonical YXXΦ endocytic motifs, we generated a cell line that stably expressed a dominant-negative μ2 subunit deficient in binding of tyrosine-based endocytic motifs. In these cells there was a strong inhibition of $P2X_4$ receptor endocytosis and an increase in surface $P2X_4$ receptor expression. The non-canonical YXXGL motif described here is present in other ion channels and receptors and may be important in their recycling and maintenance of surface expression.

Bobanovic, L.K. *et al.* (2002). *J. Neurosci.* **22**, 4814–4824.

All procedures accord with current UK legislation.

Differential release of adenosine during hypoxia in areas stratum radiatum and stratum oriens of rat hippocampus *in vitro*

B.G. Frenguelli*, E. Llaudet† and N. Dale†

**Department of Pharmacology and Neuroscience, University of Dundee, Ninewells Hospital, Dundee DD1 9SY and †School of Biological Sciences, University of Warwick, Coventry CV4 7AL, UK*

The release of adenosine during metabolic or traumatic insults to the mammalian CNS is regarded as an important neuroprotective strategy by virtue of the resultant adenosine A_1 receptor-mediated inhibition of glutamate release. We have previously shown, using an enzyme-based adenosine sensor, the production of adenosine coincident with the depression of glutamatergic synaptic transmission in s. radiatum of area CA1 of the rat hippocampus (Dale *et al.* 2000). We now present evidence that the release of adenosine in area CA1 during hypoxia is not uniform and instead shows regional variation.

Hippocampal slices were prepared from rat pups of either sex aged between 11 and 25 days as previously described (Dale *et al.* 2000). Briefly, rats were killed by cervical dislocation in accordance with Schedule 1 of the UK Animals (Scientific Procedures) Act, 1986. Hypoxia (33–34°C) was induced by switching from ACSF saturated with 95 % O_2 and 5 % CO_2 to ACSF saturated with 95 % N_2 and 5 % CO_2. Adenosine release was measured in real-time in s. radiatum and s. oriens with microelectrode sensors (25–50 μm diameter) either laid on the surface of each area or inserted through the entire depth of each region at a steep angle. Data are expressed as means ± S.E.M. and n = number of slices.

Hypoxia (5–10 min) reliably evoked adenosine release in both s. radiatum and oriens. In pups aged 11–15 days the adenosine release in s. radiatum and oriens was almost simultaneous. The difference in timing of release between the two areas (s. radiatum to oriens) was 12 ± 9 s (n = 7). In contrast, in pups 19 days or older the onset of adenosine release in s. oriens was delayed with respect to s. radiatum by 63 ± 16 s (n = 6). However, the amount of adenosine recorded in the two areas after 5 min of hypoxia was similar and did not alter with age (10 ± 4 and 8 ± 3 μM, s. radiatum and oriens, respectively). To test if adenosine is produced in both areas or only in s. radiatum and diffuses to s. oriens, we made a cut just above s. pyramidale, which enabled s. oriens to be moved away from s. radiatum. Under these conditions the amount of adenosine produced in s. radiatum after 5 min of hypoxia was 9 ± 2 μM while that in the displaced s. oriens was 0.2 ± 0.1 μM (n = 7). We conclude that, in contrast to s. radiatum, little adenosine is released in s. oriens during hypoxia. The adenosine detected in s. oriens probably arises through diffusion through the slice of adenosine released in s. radiatum or pyramidale. This surprising result challenges the assumption that a global signal such as hypoxia elicits a global, uniform release of adenosine.

Dale, N. *et al.* (2000). *J. Physiol.* **526**, 143–155.

All procedures accord with current UK legislation.

Plasticity of α4 and δ $GABA_A$ receptor subunit expression in the periaqueductal grey matter during the oestrous cycle in the rat

J.L. Griffiths, I.L. Martin* and T.A. Lovick

*Department of Physiology, University of Birmingham, Birmingham B15 2TT and *Department of Pharmaceutical Sciences, University of Aston, Birmingham B4 7ET, UK*

Neuroactive steroids such as the progesterone metabolite allopregnanolone act as positive allosteric modulators at $GABA_A$ receptors (Harrison *et al.* 1987). Changes in steroid levels can modulate $GABA_A$ receptor subunit expression and it has been shown that abrupt withdrawal from chronic progesterone treatment *in vivo* and *in vitro* is associated with increased levels of the α4 subunit in hippocampal, cortical and cerebellar tissue (Smith *et al.* 1998; Follesa *et al.* 2001). Whether the normal cyclical variations in progesterone levels that occur in females influence $GABA_A$ receptor subunit expression is not known. In the present study we have investigated immunostaining for α4 and δ $GABA_A$ receptor subunits in neurones in the periaqueductal grey matter (PAG), a region involved in producing panic-like anxiety states, in female rats at different stages of the oestrous cycle and in male rats.

Twenty female and five male 200–240 g urethane-anaesthetised (0.5–0.7 ml 100 g^{-1} 20 % solution I.P.) Wistar rats were used. The hormonal status of the females was determined from vaginal cytology. All rats were humanely killed by perfusion with 100 ml heparinised (100 U ml^{-1}) 165 mM NaCl at 30 °C followed by 200 ml 4 % paraformaldehyde in 0.1 M phosphate buffer (PB), pH 7 at 20 °C. The brain was removed and cryoprotected in 30 % sucrose in PB at 4 °C overnight. Frozen coronal sections of midbrain 40 μm thick were processed to reveal immunoreactivity for α4 and δ $GABA_A$ receptor subunits using antibodies SC-7355 N-19 and SC-7367 C-20, respectively (Santa Cruz Biotechnology).

α4 and δ subunit-immunopositive neurones were present throughout the PAG at all rostro-caudal levels. α4 subunit-stained cells were polygonal (> 75 %) fusiform or triangular with a mean diameter, measured along the longest axis, of 14.6 ± 0.4 μm (S.E.M.). δ subunit-stained cells were similar in shape and size (mean diameter 15.5 ± 0.5 μm). The density of immunopositive cells was counted within the dorsal (D), dorsolateral (DL), lateral (L) and ventrolateral (VL) sectors of the PAG. In late dioestrus, when progesterone levels fall sharply, the number of α4 immunoreactive cells increased significantly above the numbers counted at other stages of the cycle or in male rats. The increase was greatest in the DL sector. δ subunit-immunopositive cells in the DLPAG did not change significantly during the oestrous cycle.

Table 1. Immunopositive neurones per 150 000 μm^2 in the dorsolateral PAG

	α4 subunit	δ subunit
Pro-oestrus	120 ± 20.1	86 ± 17.7
Oestrus	178 ± 29.8	87 ± 25.7
Early dioestrus	106 ± 26.6	68 ± 10.3
Late dioestrus	261 ± 12.7†	114 ± 33.7
Male	168 ± 21.8	175 ± 21.1*

All values are means ± S.E.M. †Significantly different from other α4 groups. *Significantly different from pro-oestrus, oestrus and early dioestrus δ groups. $P < 0.05$, Student's unpaired *t* test.

Thus increases in α4 subunit expression in the PAG when progesterone levels fall could contribute to the increases in anxiety experienced on some women during the late luteal phase of the menstrual cycle (equivalent to late dioestrus).

Follesa, P. *et al.* (2001). *Brain Res. Rev.* **37**, 81–90.
Harrison, N.L. *et al.* (1987). *J. Neurosci.* **7**, 604–609.
Smith, S. *et al.* (1998). *J. Neurosci.* **18**, 5275–5284.

This work was supported by the British Heart Foundation.

All procedures accord with current UK legislation.

Pre-steady-state and transport-associated currents in the GABA cotransporter rGAT1 are simply related

Antonio Peres, Stefano Giovannardi, Francesca Binda, Elena Bossi and Riccardo Fesce

Laboratory of Cellular and Molecular Physiology, Department of Structural and Functional Biology, University of Insubria, Via Dunant 3, 21100 Varese, Italy

The possibility of heterologous expression of ion-dependent cotransporters has revealed that they characteristically display two kinds of membrane current: a pre-steady-state (I_{pre}) current in the absence of organic substrate, and a transport-associated (I_{tr}) current in its presence (Bossi *et al.* 1999; Forlani *et al.* 2001). A thorough comparison of these two currents elicited by the neuronal GABA transporter rGAT1 expressed in *Xenopus* oocytes leads to a number of unforeseen qualitative and quantitative consistencies between them. In saturating amounts of GABA, the following relation holds: $I_{tr} = Q_{in}r$, where Q_{in} is the quantity of charge in the inner side of the transporter, obtained in the absence of GABA from integration of I_{pre}, and r is the relaxation rate of I_{pre} at the same membrane potential (see Fig. 1).

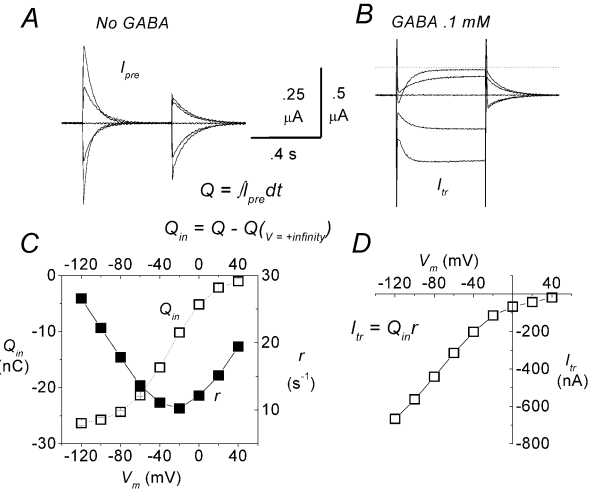

Figure 1. *A*, I_{pre} in response to voltage pulses to −120, −80, 0 and +40 mV from $V_h = -40$ mV, after subtraction of the corresponding records in presence of SKF89976A. *B*, I_{tr} in response to the same voltage protocol as in *A*, after subtraction of the corresponding records in absence of GABA; the dotted line indicates 0 current. *C*, □ are the Q_{in}/V curve obtained from integration of the transients in *A* and vertically offset, in order to make it start from 0 at positive values; fitting the sigmoidal with a Boltzmann function gives in this oocyte $Q_{max} = 26.7$ nC, $V_{½} = -30.3$ mV and log-slope $s = 21.2$ mV; ■ represent the charge equilibration rate obtained by fitting the traces in *A* with single exponentials. *D*, steady-state I_{tr} *vs.* *V* curve from records in *D*. All data are from the same oocyte.

The relation remains valid when $[Na^+]_o$ and $[Cl^-]_o$ are changed. At non-saturating GABA, decreases in the amplitude of I_{tr} are compensated by complementary variations in Q_{in}. Complementarity of magnitude, superimposable kinetic properties and dependence on V_m and $[Na^+]_o$, point to the unicity of the charge carrier for both processes. The partition of the molecule between the transporting and non-transporting forms is in agreement with the apparent affinity for the organic substrate, previously estimated from the GABA concentration eliciting half-maximal I_{tr} at each potential. The system may be simulated by a simple three-state kinetic scheme in which GABA must bind after Na^+. On the whole, these observations suggest that transport and charge migration in rGAT1 arise from the same molecular mechanism.

All experiments were carried out according to the institutional and national ethical guidelines; frogs were anaesthetized in MS222 (tricaine methansulfonate) 0.10 % (w/v) solution in tap water before oocyte dissection and humanely killed at the end of the experiments.

Bossi, E. *et al.* (1999). *J. Physiol.* **515**, 729–742.

Forlani, G. *et al.* (2001). *J. Physiol.* **536**, 479–494.

We are grateful to Professor H.A. Lester and C. Labarca for the generous gift of rGAT cDNA. This work was supported by a PRIN grant from the Italian Ministry for University and Research to A. Peres.

Changes in Ca^{2+} homeostasis during neuronal ageing are associated with changes in mitochondrial status in mouse cerebellar brain slices

Jie Xiong, Alex Verkhratsky* and Emil C. Toescu

*Department of Physiology, Division of Medical Sciences, University of Birmingham, Edgbaston, Birmingham B15 2TT and *School of Biological Sciences, University of Manchester, 1.124 Stopford Building, Oxford Road, Manchester M13 9PT, UK*

Ageing is a process associated with both neurological and psychological dysfunctions (Rubin *et al.* 2000). One of the theories that has been proposed to explain such changes is the 'calcium hypothesis of ageing', in which changes in any Ca^{2+} homeostatic mechanism would alter the neuronal physiology (Verkhratsky & Toescu, 1998). Mitochondria are intracellular organelles that sustain cellular energetics and are also intimately related to Ca^{2+} homeostasis.

In the present work, we investigated the relationship between mitochondrial function and Ca^{2+} homeostasis in brain slices obtained from mice (CB57Bl/6) that aged normally and were humanely killed in accordance with UK legislation (Schedule I). Parasagittal slices of mouse cerebellum, 250 μm thick, were cut in ice-cold artificial cerebrospinal fluid (ACSF) containing (mM): NaCl, 118; KCl, 4.7; $CaCl_2$, 2.5; $NaHCO_3$, 25; KH_2PO_4, 1.2; $MgSO_4$, 1.2; glucose, 11; equilibrated continuously with 95 % O_2 and 5 % CO_2, to maintain the pH at 7.4. During cutting and for the initial period of equilibration (30 min), the ACSF medium was supplemented with 225 mM sucrose to reduce the level of neuronal damage. After 30 min, the slices were transferred to a slice-holding chamber in which they were maintained for different periods of time until use. For Ca^{2+} measurement the slices were loaded with fura-2AM. For monitoring mitochondrial membrane potential, we have used rhodamine 123 (Toescu & Verkhratsky, 2000). Images were captured (rate 0.2–3 Hz) and analysed using an intensified GenIV camera (Roper Instruments, UK), fed from a monochromator (Cairn Research Ltd, UK), controlled through the MetaFluor software (Universal Imaging, Inc., USA). The emission was set with a 525 ± 25 nm cut-off filter (Chroma, USA) placed in a Sutter filterwheel installed in front of the camera.

When slices were stimulated (KCl depolarisation) there were significant differences in the type of patterns of Ca^{2+} signal displayed by the young and old cerebellar granule neurones (90 % of the young neurones responded with a single monophasic $[Ca^{2+}]_i$ increase, whereas only 55 % of the aged neurones responded in a similar manner. The remainder of the aged neurones showed smaller or no $[Ca^{2+}]_i$ increases and rapid $[Ca^{2+}]_i$ dysregulation following the cessation of stimulation). More importantly, the aged neurones showed a significant delay in their capacity to recover the resting $[Ca^{2+}]_i$ (recovery to 75 % of resting levels after cessation of stimulation: 1.35 ± 0.22 min in young neurones and 2.95 ± 0.45 min for the aged neurones (mean ± S.E.M.; $n = 19$ and 15 neurones for the two ages, respectively, $P < 0.001$)). In both young and aged neurones, the cytosolic $[Ca^{2+}]_i$ signal was associated with a mitochondrial depolarisation response. In the aged neurones, the mitochondria had a significantly longer repolarization response and quantitative analysis showed a direct correlation between the delays in mitochondrial repolarization and $[Ca^{2+}]_i$ recovery, indicating a causal relationship between the two parameters.

The present results thus show that the reported changes in Ca^{2+} homeostasis associated with ageing, which are manifested principally in a decreased capacity of recovering the resting $[Ca^{2+}]_i$ values after stimulation, are mainly due to a metabolic dysfunction in which mitochondrial impairment plays an important role.

Rubin, E.H. *et al.* (2000). *Res. Pract. Alzheimer Dis.* **3**, 19–33.

Toescu, E. & Verkhratsky, A. (2000). *Pflügers Arch.* **440**, 941–947.

Verkhratsky, A. & Toescu, E. (1998). *TINS* **21**, 2–7.

The financial support of BBSRC (SAGE Initiative) is gratefully acknowledged.

All procedures accord with current UK legislation.

Visualization of calcium microdomains in the synaptic terminal of goldfish bipolar cells using evanescent wave microscopy

Vahri Beaumont and Leon Lagnado

MRC Laboratory of Molecular Biology, Hills Road, Cambridge CB2 2QH, UK

Inositol 1,4,5-trisphosphate (IP_3) release mimics the inhibitory type 1 metabotropic glutamate receptor (mGluR) response in rat CA1 hippocampal neurones in acute slices

Laura Nelson and David Ogden

Neurophysiology, National Institute for Medical Research, The Ridgeway, Mill Hill, London NW7 1AA, UK

Activation of postsynaptic mGluR modifies the excitability of CA1 pyramidal neurones. The aim here was to identify the conductance changes and underlying ion channels activated by mGluR following extracellular photolytic release of L-glutamate, and to investigate the intracellular mechanisms by comparison with effects of intracellular photorelease of IP_3.

CA1 pyramidal cells in hippocampal slices from humanely killed 12-day rats were whole-cell voltage clamped, usually with potassium gluconate-based internal solution. $[Ca^{2+}]_i$ was monitored photometrically with low-affinity indicator fura-2FF. Extracellular photolytic release of L-glutamate was over an area of 200 μm diameter in 1 ms with a near UV flashlamp pulse from nitroindolinyl (NI) or methoxynitroindolinyl (MNI)-L-glutamate (Canepari *et al.* 2001). Intracellular IP_3 was released from the P5 1-(2-nitrophenylethyl) ester of IP_3 (Walker *et al.* 1989). Photolysis calibrations were as described in Canepari *et al.* (2001). Ionic currents were identified pharmacologically or by ion substitution.

The mGluR response was isolated from the ionotropic response by high concentrations of AMPA-kainate and NMDA-R antagonists, 100 μM NBQX and 400 μM D-AP5 or 200 μM CPP. The mGluR response activated within 1 s after L-glutamate release and was blocked by 1 mM MCPG. L-Glutamate concentrations of 30–50 μM resulted in mGluR responses that comprised two components, an early component that reversed at +5 mV and displayed voltage sensitivity, peak current occurring at around −30 mV. The late component reversed at −70 mV. Ion substitution indicated a potassium-selective channel and there was a coincident rise of $[Ca^{2+}]_i$ associated with this component. Furthermore, the conductance was blocked by 14 mM TEA, 100 nM apamin, but not 100 nM iberiotoxin, indicating that it is likely to be a small conductance calcium-activated potassium channel.

Antagonists acting selectively at different mGluR-subtypes (CpCCOEt 20 μM, MCCG 1 mM) indicated that the late potassium conductance is linked to activation of a Group I mGluR and the early conductance to a Group II mGluR.

The possibility that IP_3-evoked Ca^{2+} release from stores might underlie the late mGluR1 conductance was tested with photorelease of IP_3. This generated a characteristic rise of $[Ca^{2+}]_i$ associated with a potassium current that resembled the late mGluR current in time course and amplitude. The reversal potential of this current was −70 mV and it was blocked by antagonists 14 mM TEA and 100 nM apamin. Ion substitution identified a potassium conductance. The apparent affinity for IP_3 was $K = 12$ μM and responses were seen at 1–2 μM, compared with 0.2 μM in autonomic tissues and 9 μM in Purkinje neurones (Ogden & Capiod, 1997). The IP_3-evoked $[Ca^{2+}]_i$ increase was suppressed but not enhanced by prior $[Ca^{2+}]_i$ elevation by depolarisation, as found in Purkinje neurones.

Calcium appears to activate a potassium conductance, possibly due to small-conductance potassium channels. These act to inhibit neuronal excitability, by polarising the membrane towards E_K and opposing excitation via fast transmission. Thus the photorelease of IP_3 mimics the late component of the mGluR response, both in $[Ca^{2+}]_i$ increase and activation of the potassium conductance, indicating that the PI pathway mediates the late inhibitory mGluR1 response.

Canepari, M. *et al.* (2001). *J. Neurosci. Meth.* **112**, 29–42.
Ogden, D. & Capiod, T. (1997). *J. Gen. Physiol.* **109**, 741–756.
Walker, J.W. *et al.* (1989). *Biochemistry* **28**, 3272–3280.

We thank G. Papageorgiou, J.E.T. Corrie and D.R. Trentham for caged reagents.

All procedures accord with current UK legislation.

Changes in the properties of NMDA receptor-mediated EPSCs during development of mouse cerebellar Golgi cells

M.H.S. Mok, S.-Q.J. Liu and S.G. Cull-Candy

Department of Pharmacology, University College London, London WC1E 6BT, UK

We have examined the changes in the pharmacological properties and decay kinetics of NMDAR-mediated EPSCs during development of cerebellar Golgi cells. NMDARs are heteromeric assemblies containing NR1- and at least one type of NR2-subunit (NR2A-D). *In situ* hybridisation studies of the cerebellum have indicated that mRNA expression of the four NR2-subunits differs between cell types and is developmentally regulated (Watanabe *et al.* 1994). The deactivation kinetics and pharmacological properties of NMDAR-mediated currents are dependent on the type of NR2-subunit contributing to the assembly (see Cull-Candy *et al.* 2001). For example, acceleration of the NMDAR-EPSC that occurs during development at various central synapses is thought to reflect an NR2B to NR2A switch.

We examined spontaneous EPSCs in Golgi cells under whole-cell patch-clamp in thin slices from humanely killed animals (Misra *et al.* 2000). Currents were recorded at −80 mV in Mg^{2+}-free solution containing GABA- and glycine receptor blockers. EPSCs evoked by parallel fibre stimulation were also examined. At postnatal day 7 (P7), the mean decay time constant of spontaneous NMDAR-EPSCs was 72.0 ± 5.4 ms (mean ± S.E.M., $n = 11$). By P15 this was significantly reduced, with a time constant of 46.0 ± 6.0 ms ($n = 22$; $P < 0.01$, Student's unpaired t test). This speeding up of the decay kinetics suggests an increased contribution of the NR2A subunit at P15. We further investigated the possible developmental change in the contribution of NR2B and NR2A to the NMDAR-EPSC by using NR2 subunit-selective drugs. Ifenprodil selectively inhibits NR1/NR2B receptors, and the Zn^{2+} chelator *N,N,N′,N′*-tetrakis-(2-pyridylmethyl)-ethylenediamine (TPEN) is known to potentiate currents through NR1/NR2A receptors. TPEN (1 μM) had little effect at P7, but significantly augmented EPSCs by P15 (38 ± 12 % of control, $n = 7$; $P < 0.01$, paired t test). On the other hand, inhibition by 10 μM ifenprodil was significantly reduced from 71 ± 3 % at P7 ($n = 11$) to 42 ± 8 % by P15 ($n = 7$; $P < 0.01$, unpaired t test). We found a clear correlation between the faster decay time of NMDAR-EPSCs and the reduction in ifenprodil block observed during development. Similar developmental changes in decay kinetics and pharmacology were observed with parallel fibre-evoked EPSCs. It is of note that by P35 spontaneous NMDAR-EPSCs were reduced in amplitude to 35 % of that at P7.

In conclusion, our data on the pharmacological and kinetic properties of NMDAR-EPSCs indicate a developmentally regulated reduction in the contribution of NR2B- and an increasing role for the NR2A-subunit at Golgi cell synapses.

Cull-Candy, S.G. *et al.* (2001). *Curr. Opin. Neurobiol.* **11**, 327–335.
Misra, C. *et al.* (2000). *J. Physiol.* **524**, 147–162.
Watanabe, M. *et al.* (1994). *J. Comp. Neurol.* **343**, 513–519.

This work is supported by The Wellcome Trust.

All procedures accord with current UK legislation.

Developmental changes in the active membrane properties of rat intracardiac neurones *in situ*

A.A. Harper* and D.J. Adams

*School of Biomedical Sciences, University of Queensland, Queensland 4072, Australia and *Division of Molecular Physiology, University of Dundee, Dundee DD1 4HN, UK*

Direct vagal stimulation studies reveal significant decreases with postnatal age in the influence of the parasympathetic control of heart rate (Quigley *et al.* 1996). Accordingly, the electrical properties of autonomic ganglion neurones from neonatal rats appear to be different from those of mature, adult rats (Hogg *et al.* 2001).

This research aims to determine the diversity of electrophysiological properties of intracardiac ganglion neurons in a wholemount preparation of intracardiac ganglia from adult ($\geqslant 6$ weeks) and neonatal (2–5 days) Wistar rats (killed humanely in accordance with the guidelines of the University of Queensland Animal Experimentation Ethics Committee). Intracellular recordings were made using conventional sharp glass microelectrodes and the preparation was superfused with a bicarbonate-buffered physiological salt solution maintained at 37 °C.

In adult neurones, the average resting membrane potential (E_m) was -53.6 ± 1.6 mV (mean ± S.E.M., $n = 27$) and the input resistance (R_{in}) was 97.5 ± 11.5 MΩ. The E_m and R_{in} for neurones from neonatal rats was -49.5 ± 1.8 mV and 80.7 ± 17.6 MΩ ($n = 5$), which is similar to that of adult ganglion neurones.

In agreement with a previous report (Selyanko, 1992), at least two neurone types were identified in ganglia from adult rats according to the duration of the after-hyperpolarization (duration to 50 % recovery, AHP_{50}); neurones which display a brief AHP_{50} (< 30 ms) following somatic action potentials (20.9 ± 2.0 ms, $n = 10$) and long duration $AHP_{50} > 50$ ms (68.1 ± 5.1 ms, $n = 6$). This difference was significant ($P < 0.001$, unpaired t test). There was, however, no significant difference in the AHP amplitude between these groups (-14.0 ± 1.3 and -15.6 ± 1.5 mV) for brief and long duration AHP_{50} groups, respectively.

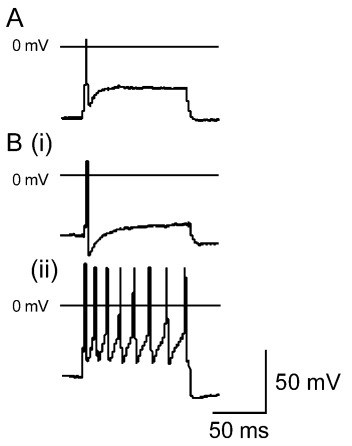

Figure 1. Representative traces of discharge activity recorded from neonatal (A) and adult (Bi, ii) rat intracardiac neurones in response to depolarizing current pulses (0.5 nA, 100 ms).

In neonatal rat intracardiac neurones, the AHP was shallow (-5.3 ± 1.6 mV, $n = 3$) and of only short duration (AHP_{50} 23.4 ± 8.3 ms).

Neonatal neurones ($n = 5$) discharged a single action potential in response to long duration depolarizing currents, whereas adult neurones exhibited a diversity of responses from fast adapting to sustained discharge (see Fig. 1).

Hogg, R.C. *et al.* (2001). *J. Neurophysiol.* **86**, 312–320.

Quigley, K.S. *et al.* (1996). *J. Auton. Nerv. Syst.* **59**, 75–82.

Selyanko, A.A. (1992). *J. Auton. Nerv. Syst.* **39**, 181–190.

A Travel award from The Wellcome Trust to A.A.H. and NHMRC grants to D.J.A. supported this work.

All procedures accord with current local guidelines.

Activation of β-adrenergic receptors enhances timing based long-term potentiation (LTP) at CA1 synapses

H.-W. Yang*, Y.-W. Lin†, C.-D. Yen† and M.-Y. Min†

Department of Life Sciences, Chung-Shan Medical University, Taichung 402 and †Department of Physiology, Chinese Medical College, Taichung 404, Taiwan

Although activation of β-adrenergic receptors has been reported to enhance homosynaptic plasticity at hippocampal CA1 synapses (Katsuki *et al.* 1997), its role in modulating the timing-based heterosynaptic plasticity received less attention. We therefore wish to address this issue in this study. Male Sprague-Dawley rats (100–150 g) were killed by cervical dislocation in accordance with the guidelines of local ethical committee for animal studies, and transverse hippocampal slices (450 μm) obtained. A recording pipette filled with 3 M NaCl was placed in stratum radiatum of the CA1 area; on both sides, two stimulating electrodes were positioned to recruit two separate Schaffer collateral pathways. The intensity of stimulation was adjusted to elicit 30–40 % of maximum response at one (weak) pathway and 80–90 % at the other (strong) pathway. Data are expressed as means ± S.E.M. and significance was tested using a paired t test.

Baseline fEPSPs of the weak pathway were evoked every 30 s for at least 10 min, and LTP of this pathway was induced by pairing the weak stimulus with the strong pathway, the weak pathway leading by 3 to 40 ms, for 100 times at 0.167 Hz. As can be seen in Fig. 1, weak–strong pairing with 3 and 10 ms delay could respectively induce LTP of 176 ± 24 % ($P < 0.001$, $n = 6$, Fig. 1*A*) and 202 ± 15 % ($P < 0.001$, $n = 6$; Fig. 1*C*). This form of LTP was NMDA dependent, as 50 μM D,L-APV blocked its induction (106 ± 6.5 %, $n = 6$; Fig. 1*A*). However, no LTP was observed if the weak–strong pairing delay was longer than 15 ms (Fig. 1*C*). Bath application of 1 μM isoproterenol (ISO) together with pairing of 15 ms delay, a protocol that produced no LTP in control conditions (109 ± 9.2 %, $n = 6$; Fig. 1*B*), resulted in LTP (185 ± 22 %, $P < 0.001$, $n = 6$). Application of ISO had no effect on the magnitude of LTP induced by pairing with 10 ms delay (177 ± 18 %, $n = 6$, ANOVA test). Taken together, the above results suggested that the window for timing-based LTP induction at CA1 synapses is of about 3–10 ms (see also Bi & Poo, 1998). Activation of β-adrenergic receptors could enhance timing based LTP by increasing the window for its induction rather than its magnitude.

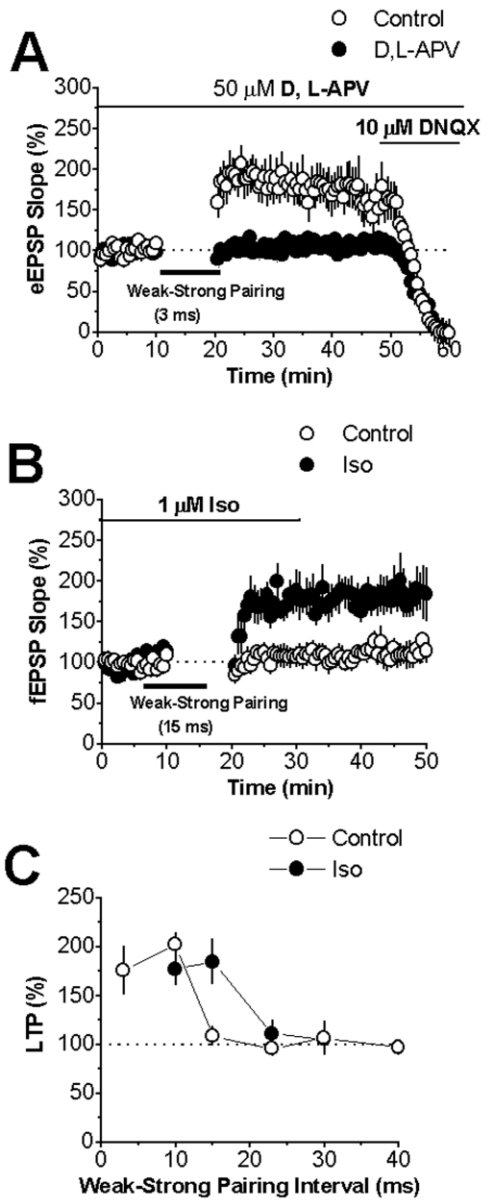

Figure 1. A, NMDA-dependent LTP of weak pathway induced by weak–strong pairing with 3 ms delay. *B*, weak–strong pairing with 15 ms delay produced no LTP in control condition, while significant LTP was induced using the same pairing protocol upon application of 1 μM ISO. *C*, window for induction of timing-based LTP in control condition, and note that it is increased upon activation of β-adrenergic receptors.

Bi, G.-Q. & Poo, M.-M. (1998). *J. Neurosci.* **18**, 10464–10472.

Katsuki, H. *et al.* (1997). *J. Neurophysiol.* **77**, 3013–3020.

This work was supported by NSC and CMC Hospital.

All procedures accord with current local guidelines.

Single-channel properties of AMPA- and kainate-receptors in CA1 pyramidal neurones of rat hippocampal slices

C. Gebhardt and S.G. Cull-Candy

Department of Pharmacology, University College London, London WC1E 6BT, UK

Non-NMDA-type glutamate receptors play a fundamental role in fast excitatory transmission at many central synapses. While much is known about the macroscopic properties of AMPA receptors in hippocampal CA1 cells (Spruston *et al.* 1995), the single-channel properties of their AMPA- and kainate (KA)-receptors have received less attention. Because of this, it has been difficult to relate the properties of synaptic non-NMDA channels with single-channel behaviour in these cells.

Steady-state recordings of single-channel currents were obtained by applying glutamate (Glu), AMPA or KA, to outside-out patches from CA1 cells in rat hippocampal slices from humanely killed animals. Two types of events were apparent in the presence of these agonists: short duration events with open-times < 500 μs, and long duration events with open times > 1 ms. Whereas both types of event could be blocked with the non-NMDAR antagonist CNQX, long duration openings were more sensitive to the AMPAR-selective blocker GYKI, suggesting that they arose from AMPARs. Consistent with this idea, we found differences between the channel openings activated by KA and AMPA/Glu. A majority of events activated by 30–100 μM KA were short duration type; the small percentage (< 10 %) of long duration events activated by KA gave a mean open time of 1.2 ms ($n = 3$ patches). On the other hand, AMPA and Glu activated predominantly long duration openings with open times up to 50 ms (mean ± S.D. 3.8 ± 0.8 ms, $n = 4$). The majority of conductance levels activated by Glu, AMPA and KA were in the range 4–10 pS; other conductance levels were also discernible but less frequent. However, at high glutamate concentrations (10–20 mM), channel openings with slope conductances of 13.6 and 16.6 pS became prevalent. During an individual long duration opening, channels displayed up to four different conductance levels. Other levels were also apparent within recordings. This suggests either that additional channel types were present or that channels could open to other levels.

In conclusion, we have identified two functionally distinct types of non-NMDAR channel in CA1 cells. The conductance values we have obtained from directly resolved single AMPAR channels are consistent with estimates of weighted mean channel conductance derived from non-stationary fluctuation analysis of glutamate-evoked responses in patches (~10–12 pS; Spruston *et al.* 1995; Banke *et al.* 2000), and estimates from synaptic AMPAR channels (4–10 pS; Benke *et al.* 1998) in these cells.

Banke, T.G. *et al.* (2000). *J. Neurosci.* **20**, 89–102.

Benke, T.A. *et al.* (1998). *Nature* **393**, 793–797.

Spruston, N. *et al.* (1995). *J. Physiol.* **482**, 325–352.

This work was supported by The Wellcome Trust.

All procedures accord with current UK legislation.

Evidence from channel properties and pore-blocking drugs that glutamate channel δ 2 underlies the metabotropic slow EPSP in cerebellar Purkinje neurones

Marco Canepari, Tomas C. Bellamy, Abdul Sesay, Chris Magnus, Thomas Kuner* and David Ogden

*National Institute for Medical Research, London NW7 1AA, UK and *Max-Planck-Institute for Medical Research, Jahnstr. 29, D-69120 Heidelberg, Germany*

The slow EPSP in Purkinje neurones (PN) due to activation of mGluR1 receptors at parallel fibre synapses is mediated by a non-selective cation channel (Canepari *et al.* 2001). mGluR1 sEPSCs were activated by photorelease of L-glutamate in 20-day rat cerebellar slices in 0.1 mM AMPAR antagonist NBQX. Biophysical and pharmacological characteristics of the sEPSC channel were compared with those of recombinant 'lurcher' GluRδ_2 channels. In PN, noise analysis gave a single channel conductance of 0.21 pS and low open probability at the peak sEPSC. Moreover, Ca^{2+} imaging with Ca^{2+} channels and PLC blocked showed the sEPSC channel is permeable to Ca^{2+}. The PN mGluR1 conductance was not affected by divalent cations that block cyclic nucleotide-gated channels, nor the I_H blocker ZD1722, nor the purinergic blocker PPADS, nor the TRP channel blocker Gd^{3+} (0.01 mM internally, 0.1 mM externally), nor TrKB blocker K252a. It was blocked by the pore-blockers naphthylacetyl spermine (0.1 mM) and adamantane derivatives IEM 1460 (Magazanik *et al.* 1997) or rimantadine (0.1–1 mM) in a use-dependent manner. The NMDA blocker MK801 (0.1 mM) and local anaesthetic nAChR blocker QX314 (0.2 mM) had no effect. Linolenic acid (0.02 mM), which blocks kainate channels, blocked the mGluR1 response. This suggests that an unedited AMPA-kainate glutamate channel underlies the sEPSP.

GluRδ_2 are present at high density in PN spines at parallel fibre synapses. For comparison of pore properties with the PN mGluR1 channel, the constitutively active Ca^{2+}-permeable 'lurcher' mutation of GluRδ_2 was tested in HEK cells (Wollmuth *et al.* 2000). The single channel conductance was 0.3 pS and the open probability low, < 10 %, at 2 mM Ca^{2+}, similar to the PN channel. The results with pore blockers were also similar to the PN sEPSC; naphthylacetylspermine and the adamantane derivatives showed open channel block at 0.1–0.5 mM, linolenic acid blocked at 0.02 mM, and MK801, QX314 and mGluR1 blocker CPCCoEt (0.02 mM) were ineffective in GluRδ_2.

The similar biophysical and pharmacological properties, and the ineffectiveness of blockers of other candidate channels present in Purkinje neurones, strongly supports the proposal that the ion channel underlying the sEPSP in cerebellar Purkinje neurones is the Ca^{2+}-permeable GluRδ_2.

Canepari, M. *et al.* (2001). *J. Physiol.* **533**, 765–772.

Magazanik, L.G. *et al.* (1997). *J. Physiol.* **505**, 655–663.

Wollmuth, L.P. *et al.* (2000). *J. Neurosci.* **20**, 5973.

We thank J. Corrie and G. Papageorgiou for NI-caged glutamate.

All procedures accord with current local guidelines.

Modulation of $GABA_A$ receptor-mediated currents by derivatives of benzophenone

M.V. Kopanitsa*, L.M. Yakubovska†, O.P. Rudenko‡ and O.A. Krishtal*

**Department of Cellular Membranology, Bogomoletz Institute of Physiology, Kyiv 01024, Ukraine, †Department of Chemistry of Biologically Active Substances, Bogatsky Physico-Chemical Institute, Odessa 65080, Ukraine and ‡Laboratory of Synthesis of Medicinal Preparations (PNIL-5), Mechnikov Odessa National University, Odessa 65058, Ukraine*

Derivatives of benzophenone occur in blood as physiological metabolites of 1,4-benzodiazepines. Some of them were shown to modulate the amplitude and time course of currents mediated by activation of $GABA_A$ receptors (Kopanitsa *et al.* 2001; Kopanitsa & Rudenko, 2002). Here we have investigated the mechanism of this modulation on the example of 5-bromo-2′-chloro-2-aminobenzophenone (BZP1), a metabolite of phenazepam, and the relationship between the chemical structure and extent of modulation of $GABA_A$ receptors among several other derivatives of benzophenone.

Whole-cell voltage-clamp recordings were obtained from individual Purkinje neurones enzymatically isolated from rat cerebellar slices (11- to 14-day-old animals rapidly decapitated according to the Institute's regulations). Drug-containing solutions were applied by the 'concentration-clamp method'. BZP1 caused dual modification of peak amplitudes of GABA-gated currents that depended upon the concentration of applied GABA and incubation time. Following short 10 s pre-incubations, 1–30 μM BZP1 facilitated activation and delayed deactivation of currents evoked by 500 μs pulses of 20 μM GABA. In addition, 10 μM BZP1 prominently enhanced biexponential desensitisation of currents during applications of 500 μM GABA mainly by decreasing the value of the fast time constant of the desensitisation. Continuous 6 min incubation with 10 μM BZP1 during GABA stimulation or its administration between but not during 1 s pulses of 500 μM GABA led to a gradual, partly reversible attenuation of GABA-activated currents. This inhibition was not observed when BZP1 was applied only during pulses of GABA, indicating that the blockade was not use dependent.

At concentrations of 10 μM, several 5-substituted benzophenones, but not 2-aminobenzophenone or benzophenone itself exhibited modulatory properties similar to BZP1 (accelerated activation and desensitisation, decelerated deactivation of GABA-activated currents) and distinct from those of picrotoxin (10−30 μM) and benzylpenicillin (500 μM). Therefore, we conclude that derivatives of benzophenone are a novel class of $GABA_A$ receptor modulators with unique pharmacological profile.

Kopanitsa, M.V. *et al.* (2001). *Naunyn-Schmied. Arch. Pharmacol.* **364**, 1–8.

Kopanitsa, M.V. & Rudenko, O.V. (2002). *Arch. Clin. Exp. Med.* (in the Press).

This work was supported by INTAS, The Wellcome Trust and HHMI.

All procedures accord with current local guidelines.

Whole-cell recordings of membrane currents induced by 2-deoxy-D-glucose in rat hippocampal pyramidal neurones

Hafejee Essackjee and Gul Erdemli

Physiology Department, University of Liverpool, Crown Street, Liverpool L69 3BX, UK

Temporary (10–20 min) replacement of glucose in the perfusion medium with 2-deoxy-D-glucose (2-DG) causes a marked and sustained potentiation of excitatory synaptic transmission in CA1 hippocampus (Tekkök & Krnjevic, 1995). Intracellular sharp microelectrode recordings have shown that 2-DG induces hyperpolarization accompanied by an increase in input resistance (Krnjevic & Zhao, 2000). We performed whole-cell and perforated patch-clamp experiments on CA1 pyramidal neurones and investigated the effects of 2-DG on baseline holding current (I_{BH}) and input conductance (G_N). Transverse hippocampal slices were prepared from Male Wistar rats (100–120 g) and kept submerged at 34 °C (animals were humanely killed according to UK legislation). Electrodes were filled with a solution containing (mM): $KMeSO_4$ (118), KCl (18), Hepes (10), EGTA (1), $CaCl_2$ (0.1), Mg-ATP (2-10), Na-GTP (0.3) and NaCl (8). In some experiments K_2-creatine phosphate (20 mM) and phosphocreatine kinase (50 U l^{-1}) were also added (ATP regenerating solution). In 17 cells clamped at −60 mV replacement of glucose in perfusion medium with 2-DG (10 mM for 15 min) resulted in an inward shift in I_{BH} (−1330 ± 120 pA, mean ± S.E.M.) and an increase in G_N (75 ± 11 %) ($P < 0.001$). These changes in I_{BH} and G_N did not recover upon perfusion with glucose-containing saline for 45 min ($n = 9$). In ten cells glucose was replaced with sucrose (10 mM) and similar effects on I_{BH} (−1470 ± 230 pA) and G_N (84 ± 26 %) were observed ($P < 0.001$). Increasing ATP concentration in the electrode filling solution to 10 mM ($n = 7$) or recording with ATP regenerating solution ($n = 5$) did not affect the 2-DG-induced changes in I_{BH} and G_N. In 12 cells recorded with amphotericin B-containing electrode filling solution (perforated patch) 2-DG induced similar changes in I_{BH} (−1240 ± 170 pA) and G_N (88 ± 14 %) ($P < 0.001$). A cocktail of glutamate receptor antagonists containing (μM): D(−)-amino-5-phosphonopentanoic acid (50), 7-chlorokynurenate (100), MK-801 (50) and 2,3-dioxo-6-nitro-1,2,3,4-tetrahydrobenzol[f]quinoxaline-7-sulphonamide (50) depressed the 2-DG effects on I_{BH} (−260 ± 30 pA) and G_N (12 ± 4 %) ($n = 9$) ($P < 0.01$). These results suggest that excessive glutamate accumulation may be responsible for the 2-DG-induced changes in I_{BH} and G_N in cells recorded in whole-cell or perforated patch-clamp mode.

Tekkök, S. & Krnjevic, K. (1995). *J. Neurophysiol.* **74**, 2763–2766.

Krnjevic, K. & Zhao, Y.T. (2000). *J. Neurophysiol.* **83**, 879–887.

This work is supported by BBSRC.

All procedures accord with current UK legislation.

Long-term nimodipine treatment reverses diabetes-induced changes in calcium signalling of rat nociceptive neurons

I. Kruglikov, V. Shishkin, L. Shutov, E. Kostyuk and N. Voitenko

Bogomoletz Institute of Physiology, Kiev, 01024, Ukraine

Impairment of cellular ionic homeostasis is one of the causes of several diabetic complications including neuropathies. We have previously shown certain changes of intracellular calcium signalling in nociceptive neurones in rats with streptozotocin (STZ)-induced diabetic neuropathy. In this study we have investigated possible effects of prolonged rat treatment with the L-type calcium channel blocker nimodipine on diabetic-induced changes in intracellular Ca^{2+} ($[Ca^{2+}]_i$) signalling and neuropathic symptoms.

Experiments were conducted on isolated neurones from dorsal root ganglia (DRG) and dorsal horn (DH) neurones from thin spinal cord slices of the lumbar L4–L6. Animals were anaesthetised (isofluorane) during preparative surgery and then humanely killed in accordance with the Bogomoletz Institute's animal care guidelines. Diabetes was evoked by a single I.P. injection of STZ (80 mg kg^{-1}). $[Ca^{2+}]_i$ was measured by microfluorescence technique using fura-2 and indo-1.

After 3 weeks of diabetes development young diabetic rats (6–7 weeks old) were treated with nimodipine (40 mg kg^{-1} per day) over the next 3 weeks. We examined the effects of nimodipine treatment on Ca^{2+} release from the intracellular calcium stores of DRG and DH neurones in diabetic animals compared with those observed in neurones from control and non-treated diabetic animals. Caffeine (20 mM) application to DRG neurones induced a transient elevation of $[Ca^{2+}]_i$ with an amplitude of 943 ± 73 nM ($n = 26$) in control, 357 ± 51 nM ($n = 16$) under diabetes and 796 ± 67 nM ($n = 39$) in neurones from nimodipine-treated diabetic animals. The difference in $[Ca^{2+}]_i$ elevations between control and nimodipine-treated rats was not significant ($P > 0.07$). Caffeine application to DH neurones induced $[Ca^{2+}]_i$ rise with an amplitude (nM) of 196 ± 17 ($n = 16$), 107 ± 14 ($n = 17$) and 145 ± 12 ($n = 36$) in control, diabetic and nimodipine-treated diabetic neurones, respectively. Thus in DH neurones nimodipine treatment partially restored the amplitude of responses to caffeine; the recovery is statistically significant ($P < 0.04$, Student's unpaired t test). Ionomycin (500 nM) application in Ca^{2+}-free extracellular solution induced $[Ca^{2+}]_i$ elevation in DRG neurones with amplitudes of 236 ± 20 ($n = 19$), 116 ± 26 ($n = 16$) and 238 ± 25 ($n = 32$) in control, diabetic and nimodipine-treated diabetic neurones, respectively. Nimodipine treatment completely restored to control level the amplitude of responses to ionomycin; the difference was not significant ($P > 0.95$). Nimodipine also partially reversed STZ-induced thermal hypoalgesia in diabetic rats: diabetic nimodipine-treated animals displayed increased withdrawal latency to painful thermal stimuli, when placed on a hot (48 °C) surface, compared with the non-treated age-matched diabetic rats. The results of this study suggest that chronic nimodipine treatment may be effective in reducing diabetes-induced thermal hypoalgesia, as well as in recovery of calcium-regulating mechanisms of the endoplasmic reticulum affected by diabetes.

This work was supported by JDFI and CRDF grants to N.V.

All procedures accord with current local guidelines.

2-Photon imaging of IP_3-evoked Ca^{2+} signals in mouse cortical neurons

Grace E. Stutzmann and Ian Parker

Department of Neurobiology and Behavior, University of California, Irvine, CA 92697, USA

Our knowledge of inositol trisphosphate (IP_3) as a calcium mobilizing second messenger derives primarily from studies in non-excitable cells. In contrast, less is known regarding its functions in neurons, despite the important roles played by cytosolic Ca^{2+} ions in regulating electrical excitability and synaptic plasticity (Berridge, 1998). Most studies of neuronal IP_3 signalling have focused on the cerebellum and hippocampus, and surprisingly little is known about its functions in the cerebral cortex. In this study, we analysed neurons in the prefrontal cortex, where IP_3-evoked Ca^{2+} signals are likely to exert widespread influences on sensory, motor, limbic and memory systems.

We combined *in vitro* visualized whole-cell electrophysiological recordings with 2-photon, video-rate Ca^{2+} imaging (Nguyen *et al.* 2001). Layer V pyramidal neurons from mouse brain slices were filled with the Ca^{2+} indicator fura-2 (50 μM) and caged IP_3 (50 μM). Mice were deeply anaesthetized with halothane before decapitation, in compliance with UCI IACUC regulations. Ca^{2+} responses following photorelease of intracellular IP_3 by flashes of UV light could be categorized into the following groups: (1) non-responders (no Ca^{2+} release even with strong UV flashes, 31 %, 33/106 neurons); (2) slow and weak responders (17 %); (3) brisk responders (rapid and large Ca^{2+} increase with short UV flashes, 56 %). In all responding cells, the soma demonstrated the highest sensitivity to IP_3, while release in the dendrites required either much stronger flashes, or was absent altogether (Fig. 1*A*). Interestingly, IP_3-evoked Ca^{2+} signals in many non- and weakly responding cells could be 'rescued' by evoking a train of action potentials prior to uncaging IP_3. In contrast, paired UV flashes in responders resulted in suppression of the second Ca^{2+} response. Voltage-clamp studies revealed the activation of a slow outward current following photorelease of IP_3, and UV flashes during a train of action potentials evoked by injection of inward current resulted in suppression of spikes (Fig. 1*B*).

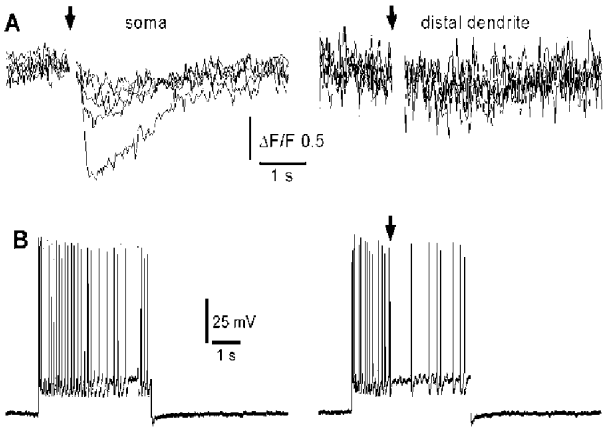

Figure 1. A, Calcium signals (decreasing fluorescence of fura-2 with 2-photon excitation at 780 nm) evoked in the soma and dendrite (50 μm distant) of a pyramidal neuron in response to photorelease of IP_3. Superimposed traces show responses to flashes with durations of 15, 20, 30, 50 and 100 ms, delivery beginning where marked by the arrows. B, photorelease of IP_3 (arrow) during a train of action potentials induced by injection of depolarizing current (0.5 nA) caused a decrease in firing rate.

These data demonstrate bi-directional interactions between intracellular IP_3-evoked Ca^{2+} release and influx of extracellular Ca^{2+} through voltage-gated channels in cortical pyramidal neurons. Ca^{2+} influx potentiates IP_3-mediated signals via mechanisms involving both a co-agonist effect on the IP_3 receptor and enhanced filling of IP_3-sensitive stores. Conversely, cytosolic Ca^{2+} elevations evoked in the soma by liberation from IP_3-sensitive stores powerfully reduce neuronal excitability by activating Ca^{2+}-dependent K^+ conductances.

Berridge, M.J. (1998). *Neuron* **21**, 13–26.

Nguyen, Q.-T. *et al.* (2001). *Cell Calcium* **30**, 383–393.

This work was supported by the NIH. G.E.S. is supported by an NIA training grant.

All procedures accord with current local guidelines

Agonist-induced modulation of cell surface cannabinoid CB1 receptors in cerebellar granule cells

Jennifer Shaw and Andrew Irving

Department of Pharmacology and Neuroscience, University of Dundee, Dundee DD1 9SY, UK

Agonist-induced internalisation of G-protein-coupled receptors is an important mechanism underlying receptor desensitisation. Recently, agonist-induced internalisation of cannabinoid CB1 receptors has been demonstrated in cultured hippocampal neurons, where the rate of down-regulation was unusually slow (5–16 h for maximal loss of labelling; Coutts *et al.* 2001). Here CB1 receptors are expressed on a subset of inhibitory synaptic terminals; however, in cultures derived from the cerebellum, they are primarily associated with excitatory synaptic terminals (Irving *et al.* 2002). In the present study, we have used an antibody directed against the N-terminal 77 amino acid residues of the cloned rat CB1 receptor (Coutts *et al.* 2001) to investigate the down-regulation of surface CB1 receptors in rat cultured cerebellar granule cells.

For cell surface labelling, cerebellar cultures were incubated with rabbit CB1 receptor antibody for 60 min (room temperature) in a standard Hepes-buffered saline; cells were then fixed with 4 % paraformaldehyde for 10 min. The CB1 receptor immunostaining was then visualised by addition of Cy3-conjugated secondary antibody. A laser-scanning confocal imaging system (Zeiss LSM 510) was used for image acquisition and processing. A minimum of nine randomly selected areas (1000 μm^2), from three experiments were used to assess total labelling (mean intensity × area of immunoreactivity). Donor animals were humanely killed.

Cell surface CB1 receptor labelling was highly punctate, with clusters decorating a network of fine neurites. Prolonged exposure (18 h, 37 °C) to the cannabinoid receptor agonist WIN55212-2 (1 μM) produced a dramatic decrease in cell surface CB1 receptor labelling (12 ± 5 % control; mean ± S.E.M.; $P < 0.01$; ANOVA), which was reversed by the selective CB1 receptor antagonist SR141617A (400 nM; to 63 ± 5 %). The time taken for CB1 receptor labelling to decrease by 50 % in the presence of agonist was 0.49 ± 0.12 h ($n = 6$). Pretreatment of the cerebellar neurons with the endocannabinoid uptake inhibitor AM404 (10 μM) also caused a marked decrease in cell surface labelling (14 ± 2 %; $P < 0.01$) and this effect was partially reversed by SR141716A (400 nM; to 57 ± 11 %), demonstrating the presence of endogenous cannabinoids in the cerebellar cultures. These findings also suggest that the rate of agonist-

induced down-regulation of neuronal CB1 receptors can vary quite profoundly between different preparations. Ultimately, this could be an important factor in the development of tolerance towards cannabinoids within the brain.

Coutts, A.A. *et al.* (2001). *J. Neurosci.* **21**, 2425–2433.
Irving, A.J. *et al.* (2002). *The Scientific World* **2**, 632–648.

This work was supported by the MRC.

All procedures accord with current UK legislation.

N-arachidonylethanolamide ('anandamide') blocks sustained repetitive firing (SRF) in rat cortical pyramidal cells independently of CB_1 receptors

Adam C. Errington and George Lees

Institute of Pharmacy, Chemistry and Biomedical Sciences, School of Sciences, University of Sunderland, Sunderland SR1 3SD, UK

Anadamide is a putative endogenous cannabinoid. It has been shown to produce the characteristic tetrad of behaviours associated with cannabinoid receptor ligands in mice. In CB_1 receptor knockout mice, anandamide is analgesic whilst the antinociceptive effects of Δ^9-THC are lost (Di Marzo *et al.* 2001). Another endocannabinoid candidate oleamide has been shown to inhibit SRF, secondary to block of the voltage-gated Na^+ channel (Verdon *et al.* 2000). Here we hypothesise that anandamide may elicit the same block.

Cultured rat cortical neurones from humanely killed animals were used after 14–21 days *in vitro*. Cells were current clamped at 24 °C and superfused with cobalt-containing saline solution into which drugs were dissolved using 0.1 % DMSO as a vehicle. Only cells with a membrane potential < -50 mV were examined. Stimuli (750 ms) sufficient to produce SRF (over-shooting action potentials) were applied at 0.1 Hz. Results are expressed as percentage of mean ± S.E.M. Analysis was by Student's unpaired *t* test and one-way repeated-measures ANOVA where appropriate. Results are expressed as percentage of residual secondary spikes at $t = 15$ min compared with 0 time in the presence and absence of drugs.

Time-matched vehicle blanks produced a small reduction in the percentage of secondary spikes (7.87 ± 6.93 %, $n = 7$). Anandamide (10 μM) produced a significant ($P = 0.012$, $n = 7$) block of 31.27 ± 4.72 % when compared with time-matched controls. At 20 μM, block was increased to 85.65 ± 10.38 % ($P = 0.0001$, $n = 4$). The block produced by 20 μM anandamide could not be inhibited by the CB_1 receptor antagonist AM251 (1 μM). 1,1,1-Trifluoro-10(Z)-nonadecen-2-one (TFNO) and phenylmethylsulphonyl fluoride (PMSF) did not significantly ($P > 0.05$) block SRF compared with control with 9.03 ± 3.66 % ($n = 4$) and 16.27 ± 11.58 % ($n = 4$) block, respectively. The percentage block produced by a suprathreshold concentration of anandamide (10 μM) could be significantly potentiated by 320 nM TFNO (71.06 ± 8.93 %; $P = 0.0009$, $n = 5$) and 100 μM PMSF (73.83 ± 11.76 %; $P = 0.002$, $n = 6$) compared with anandamide alone.

The voltage-gated Na^+ channel may underpin some of the non-CB_1-dependent effects of anadamide. FAAH limits the potency of exogenous anandamide *in vitro* and may represent an attractive target for drug design (Walker *et al.* 1999).

Di Marzo, V. *et al.* (2001). *J. Neurochem.* **75**, 2434–2444.
Verdon, B. *et al.* (2000). *Br. J. Pharmacol.* **129**, 283–290.
Walker, J.M. *et al.* (1999). *Proc. Natl Acad. Sci. USA* **96**, 12198–12203.

Thanks to The Wellcome Trust, UK and Schwarz Pharma AG, Germany for equipment support.

All procedures accord with current UK legislation.

Behavioural effects of prolyl-tyrosin-containing dipeptide in C57BL/6 mice following MPTP administration

M.N. Voukolova*, V.K. Lutsenko*, V.G. Kucheryanu* and T.A. Gudasheva†

**Institute of General Pathology and Pathophysiology RAMS, Moscow and †Institute of Pharmacology of RAMS, Moscow, Russia*

Parkinson's disease (PD) is a severe and progressive motor disorder of the central nervous system. In PD the pigmented neurons, particularly the pars compacta of the substantia nigra, are susceptible to apoptosis. The pathophysiological mechanism of cell death in PD is unknown; however, some hypotheses have been developed. This is an area where much further research is needed to find possible neuroprotective agents. The neurotoxin 1-methyl-4-phenyl-1,2,3,6-tetrahydropyridine (MPTP) can damage dopamine systems in the brains of rodents, cats or monkeys, and is therefore widely used to model degenerative processes that underlie human PD. Various neurotrophic factors and peptides are prospective in prevention of neurodegeneration processes.

The aim of the present study was to investigate the influence of a new prolyl-tyrosin-containing dipeptide (PTCD) on MPTP-induced parkinsonian syndrome (PS) in mice. This compound was synthesized at the Institute of Pharmacology of RAMS, Russia. Two experimental series were carried out on 3- to 5-month-old C57Bl/6 male mice. The first experimental series demonstrated, that mice injected with MPTP only (30 mg kg^{-1} I.P., twice daily, every 12 h for 7 days) did not survive for longer than 7 days. In mice injected with PTCD (2 mg kg^{-1} I.P.) and MPTP (30 mg kg^{-1} I.P.), survival at the 21st day was 100 %, and the animals did not show any significant symptoms of PS. Therefore, the neuropeptide protected mice against acute intoxication. In the second experimental series, mice injected with MPTP (25 mg kg^{-1} I.P.) demonstrated some symptoms of PC by the 14th day: their motor activity decreased, the rigidity increased, the time spent motionless significantly increased, and the number of vertical movements significantly decreased on the 7th and 14th days. However, in MPTP-treated mice (25 mg kg^{-1}, I.P.) with PTDC (2 mg kg^{-1}, I.P.) investigated parameters did not differ from those in control animals. The development of PS was assessed by oligokinesia and muscle rigidity. Oligokinesia was estimated by changes in the motor activity and the number of vertical movements (rearings). Motor activity was monitored, allowing us to follow the dynamics, and the total motor activity of animals was measured in an automated regime for 3 min using the 'Auto-Track' program in opto-Varimex-3 system composed of a host controller (Apple-IIe), an interface box and 16 infrared beam-based activity sensors (Columbus Instruments, USA). Our previous data indicate that PTCD increased short-term of movement activity, the number of vertical movements, and speed of horizontal movements. It reduced muscular rigidity and time spent motionless. Signs of rigidity were also different: in MPTP-treated mice rigidity reached 0.86 points on the 7th day, and 2.29 points on the 14th day, while in mice subjected to I.P. administration of PTCD, rigidity was about 0.77 and 1.33 points, respectively. MPTP administration (daily, for 14 days) caused weight loss in experimental mice. It is supposed that PTDP has a

neuroprotective effect. Preliminary data suggest that it is possible to protect DA-ergic neurons from MPTP neurotoxin with PTCD. The target for PTCD's action could be neurotoxin intracellular transport. Further studies of PTCD's mechanism of action in biochemical models are needed.

Research was supported by the RFBR grants 00-04-48391 and 02-04-06617.

All procedures accord with current local guidelines.